




 Cite this: *Nanoscale*, 2024, **16**, 1924

## A novel bifunctional multilayered nanofibrous membrane combining polycaprolactone and poly (vinyl alcohol) enriched with platelet lysate for skin wound healing†

 Andreu Blanquer,<sup>a</sup>  \*<sup>a,b</sup> Eva Kuzelova Kostakova,<sup>c</sup> Elena Filova,<sup>b</sup> Maxim Lisnenko,<sup>c</sup> Antonin Broz,<sup>b</sup> Jana Mullerova,<sup>c,d</sup> Vit Novotny,<sup>d</sup> Kristyna Havlickova,<sup>c</sup> Sarka Jakubkova,<sup>e</sup> Sarka Hauzerova,<sup>c</sup> Bohdana Heczko,<sup>e</sup> Renata Prochazkova,<sup>e,f</sup> Lucie Bacakova <sup>b</sup> and Vera Jencova<sup>c</sup>

Skin wound healing is a complex physiological process that involves various cell types, growth factors, cytokines, and other bioactive compounds. In this study, a novel dual-function multilayered nanofibrous membrane is developed for chronic wound application. The membrane is composed of five alternating layers of polycaprolactone (PCL) and poly (vinyl alcohol) (PVA) nanofibers (PCL-PVA) with a dual function: the PCL nanofibrous layers allow cell adhesion and growth, and the PVA layers enriched with incorporated platelet lysate (PCL-PVA + PL) serve as a drug delivery system for continuous release of bioactive compounds from PL into an aqueous environment. The material is produced using a needleless multi-jet electrospinning approach which can lead to homogeneous large-scale production. The bioactive PCL-PVA + PL membranes are cytocompatible and hemocompatible. A spatially compartmented co-culture of three cell types involved in wound healing – keratinocytes, fibroblasts and endothelial cells – is used for cytocompatibility studies. PCL-PVA + PL membranes enhance the proliferation of all cell types and increase the migration of both fibroblasts and endothelial cells. The membranes are also hemocompatible without any deleterious effect for thrombogenicity, hemolysis and coagulation. Thus, the beneficial effect of the PCL-PVA + PL membrane is demonstrated *in vitro*, making it a promising scaffold for the treatment of chronic wounds.

 Received 18th September 2023,  
 Accepted 3rd December 2023

DOI: 10.1039/d3nr04705a

[rsc.li/nanoscale](https://rsc.li/nanoscale)

### 1. Introduction

Skin wound healing is a complex physiological process of multiple steps that involve various cell types which proliferate and migrate to the wound site. However, not only cells play a role in wound healing. Growth factors, cytokines and other metab-

olites and ions are also necessary in the healing process.<sup>1,2</sup> The main cell types involved in skin wound healing include keratinocytes, fibroblasts, endothelial cells and immune cells. Keratinocytes are the most abundant cell type of epidermis, whereas fibroblasts and endothelial cells are present in the dermis. During the inflammatory phase of the healing process, immune cells reach the wound site and release chemoattractants and growth factors. This release of chemotactic agents and growth factors is responsible for the migration and proliferation of fibroblasts and keratinocytes. In addition, endothelial cells migrate to the wound site as an essential step to ensure wound healing and allow the formation of new capillaries. Under certain circumstances, the skin requires a long time to heal or, in cases that can be classified as chronic wounds, not to heal. Chronic wounds include pressure ulcers, venous leg ulcers, arterial ulcers, neurotrophic ulcers, and foot ulcers in people with diabetes.<sup>3</sup> The prevalence of chronic wounds increases along with vascular diseases, diabetes mellitus or advanced age. It is estimated that 1–2% of the population will experience a chronic wound during their lifetime

<sup>a</sup>Departament de Biologia Cel·lular, Fisiologia i Immunologia, Universitat Autònoma de Barcelona, Bellaterra, Cerdanyola del Vallès, 08193, Spain.

E-mail: andreu.blanquer@uab.cat

<sup>b</sup>Institute of Physiology of the Czech Academy of Sciences, Videnska 1083, 142 00 Prague 4-Krc, Czech Republic

<sup>c</sup>Technical University of Liberec, Faculty of Science, Humanities and Education, Studentska 1402/2, Liberec, 46117, Czech Republic

<sup>d</sup>The Institute for Nanomaterials, Advanced Technologies and Innovation, Bendlova 1409/7, Liberec, 460 01, Czech Republic

<sup>e</sup>Regional Hospital Liberec, Husova 357/28, Liberec, 460 01, Czech Republic

<sup>f</sup>Faculty of Health, Technical University of Liberec, Studentska 1402/2, Liberec, 461 17, Czech Republic

† Electronic supplementary information (ESI) available. See DOI: <https://doi.org/10.1039/d3nr04705a>



and, specifically, 15% of patients suffering from type 2 diabetes mellitus will develop ulcers.<sup>4,5</sup>

Chronic wounds are characterized by the imbalance of cytokines and the reduction of growth factors at the wound site. In addition, the proliferation of skin-resident cells is significantly reduced,<sup>5,6</sup> as is migration, due to the lack of chemoattractants and growth factors. In this regard, the addition of growth factors and other proteins and ions could enhance wound healing. Platelet derivatives such as platelet-rich plasma, platelet gel or platelet lysate (PL) can be used for therapeutic approaches due to the high number of bioactive compounds.<sup>7</sup> The components of platelet derivatives include coagulation factors, vasoactive factors and growth factors.<sup>8</sup> Human PL is a potential therapeutic tool highly enriched in several growth factors that play an important role in the migration and differentiation of keratinocytes, fibroblasts and endothelial cells. These factors include platelet-derived growth factor (PDGF), vascular endothelial growth factor (VEGF), epidermal growth factor (EGF) and basic fibroblast growth factor (bFGF), among others.<sup>9</sup> The use of PL as a therapeutic approach to improve chronic wound healing can be combined with the development of new wound dressings or skin scaffolds.<sup>10</sup>

Among the materials currently being developed for skin tissue engineering, nanofibrous layers have shown great promise. The nanofibrous structure is similar to the natural skin extracellular matrix, which ensures high porosity and a high surface-to-volume ratio. These specific material properties have been shown to improve cell adhesion and proliferation, reduce pathogen penetration, and help to provide a moist environment during healing.<sup>11,12</sup> Electrospinning is one of the most successful methods for the preparation of nanofibrous materials for medicine. One of the advantages is the possibility to prepare materials from polymer solutions using a wide range of natural and synthetic polymers.<sup>12,13</sup> In combination with other technologies, even large homogeneous layers can be produced,<sup>14,15</sup> and can be used as drug-delivery systems.<sup>16</sup> In addition to the choice of a polymer, the morphology of the materials can also be influenced by the technology used for production and its technological parameters. Planar nanofibrous layers with small fiber diameters are particularly suitable for the treatment of chronic and acute wounds.<sup>17</sup> In addition to their nanofibrous structure, nanofibrous membranes can be further functionalized using biologically active compounds that promote wound healing, such as growth factors.<sup>18,19</sup> For wound dressings, the use of biodegradable polymers can be advantageous, and aliphatic polyesters (e.g. polycaprolactone) are among the most commonly used.<sup>12,20,21</sup> Nanofibrous materials made from biodegradable polyesters degrade slowly, and the mechanical support for the cells can thus be stable for the required time.<sup>22,23</sup> By contrast, most polyesters are hydrophobic, and it is necessary to use aggressive organic solvents for producing them. Thus, the direct incorporation of sensitive biologically active proteins can be problematic. It is therefore advantageous to use water-soluble polymers, e.g. poly (vinyl alcohol), for the preparation of nanofibers with incorporated proteins that ensure minimal

loss of their activity.<sup>16,19</sup> By contrast, the resulting material is soluble in an aqueous environment, so the incorporated molecules are quickly released, and the fibrous structure of the material is lost. In addition, the strongly hydrophilic nature of these materials is not very suitable for cell proliferation. It could therefore be beneficial to use a material combining the advantages of the good mechanical properties of polyester fibers, whose hydrophobicity would be reduced by the presence of a hydrophilic component with incorporated growth factors. In this regard, the electrospinning of nanofibrous materials combining hydrophilic and hydrophobic polymer fibers requires special approaches. Special electrospinning devices using two or more spinning electrodes with different arrangements are used to create these materials.<sup>24,25</sup> Multi-jet electrospinning offers the possibility to spin several types of polymers at the same time to create a material containing a blend of nanofibers from these polymers. Indeed, needleless electrospinning reduces the unwanted interactions between adjacent jets that are generated by widely-used multi-needle electrospinning.<sup>25,26</sup> The combination of poly (vinyl alcohol) (PVA) and polycaprolactone (PCL) nanofibers has so far been presented only in the form of a few layers, most often two,<sup>27,28</sup> or three,<sup>29</sup> created using needle electrospinning on a rotating cylindrical collector from one nozzle successively in time or from two nozzles simultaneously – dual-jet electrospinning.<sup>30,31</sup> Such needle electrospinning requires an hour or more to prepare a sample several square centimeters in size. The needleless approach using semi-operational equipment, as presented in this article, offers the production of more uniform nanofibrous layers with higher productivity, and thus the possibility to produce larger samples.

In the present study, the biodegradable hydrophobic polyester PCL was used.<sup>32,33</sup> PCL exhibits suitable properties for use in skin tissue engineering, and has been approved by the Food and Drug Administration (FDA). Water-soluble PVA, used for skin tissue engineering, especially in the form of a hydrogel, was chosen as the second polymer, being a polymer suitable for protein incorporation.<sup>34</sup> In our previous work, PVA with a high degree of hydrolysis was used to prepare a large-scale nanofibrous layer with incorporated platelet growth factors with prolonged release of these proteins and a beneficial effect on skin cells.<sup>14,35</sup> Here, PL was incorporated into PVA to obtain a multilayered nanofibrous membrane of PCL and PVA with PL (PCL-PVA + PL) and without PL (PCL-PVA). The fabricated membrane contained PCL to allow cell adhesion and growth, while PVA acted as a hydrogel releasing bioactive substances. The novel bifunctional nanofibrous membranes combined two different materials – hydrophilic and hydrophobic – with interesting properties to be used in wound healing application. The effect of the PCL-PVA + PL membranes was evaluated *in vitro* using three skin cell types involved in wound healing, *i.e.* keratinocytes, fibroblasts and endothelial cells. The three cell types were co-cultured with the membranes to assess the behavior of the cells when cultured together and to provide a more realistic model of the situation *in vivo*. The effect of PCL-PVA + PL was compared with PCL-PVA membranes without PL and with PCL membranes.



## 2. Experimental

### 2.1. Platelet lysate (PL) preparation

A platelet concentrate was obtained *via* the centrifugation of platelets from human buffy coats of 4 donors. The experimental procedure was previously detailed in a study by Blanquer *et al.*<sup>36</sup> Briefly, the buffy coats from patients were mixed and were centrifuged to separate the platelet concentrate from the other cell types, *e.g.* leucocytes. The final platelet concentration was determined in the range of  $600 \times 10^9$  to  $850 \times 10^9$  platelets per L. Then, the PL was prepared using the freeze–thaw method to disrupt the platelets, and the subsequent centrifugation was used to remove the cellular debris. The supernatant, *i.e.* PL, was stored at  $-80$  °C.

### 2.2. Preparation and morphology characterization of nanofibrous membranes

The multilayer membranes of polycaprolactone (PCL) and poly(vinyl alcohol) (PVA) were fabricated by the direct current needleless electrospinning technique. Both polymers were purchased from Merck KGaA (Germany). Two electrospinning solutions were prepared. The PCL solution contained 16% (w/w) PCL ( $M_n$  45 000 g mol<sup>-1</sup>) in a chloroform/ethanol solution (8 : 2 (w/w)), and the PVA solution contained 10% (w/w) PVA ( $M_w$  125 000) with a 98% degree of hydrolysis in an HPLC water/ethanol solution (9 : 1). All solvents were purchased from Penta (Czech Republic). For PVA, two types of nanofibers were prepared, either containing PL or without PL. The PVA-containing PL (PVA + PL) was obtained by adding 10% w/w of PL into the spinning solution immediately before electrospinning (the procedure was described in detail in our previous work by Koprivova *et al.*<sup>14</sup>). Nanofibrous single-layer materials from

PCL and PVA solutions were produced by needleless electrospinning technology (Nanospider NS 1WS500U; Elmarco, Czech Republic) (Fig. 1a). The five-layer materials of both polymers (PCL-PVA and PCL-PVA + PL) were produced by the same device but using two spinning electrodes in the form of stationary wires (special spinning electrode modification performed at the Technical University of Liberec; Fig. 1b and c). The five-layer materials were produced in three different steps – three passes through the machine, as illustrated in Fig. 1d. Spunbond Pegatex S 20 g m<sup>-2</sup> (PF Nonwovens Czech, Czech Republic) was used as a supporting material for the preparation of all samples. The process parameters used in the production of the nanofibrous materials are presented in Table 1. The electrospinning was performed at a relative humidity and a temperature ensured by a precisely controlled air conditioning system (NS AC150; Elmarco, Czech Republic).

The morphology of the nanofibrous membranes was analyzed by scanning electron microscopy (Vega S3B EasyProbe, Tescan Orsay Holding a.s., Czech Republic) and the diameter of the fibers was evaluated from at least 360 measurements, using ImageJ software (NIH, USA).

### 2.3. Infrared spectroscopy (FT-IR) analysis

The chemical composition of materials was analyzed by attenuated total reflection Fourier transform infrared spectroscopy (ATR-FTIR), using a Fourier transform spectrometer (Nicolet iZ10, ThermoFisher Scientific, Waltham, MA, USA) at room temperature. The multi-layer membranes were placed on the ATR diamond crystal for analysis. The spectrum analysis was performed in the infrared region 400–4000 cm<sup>-1</sup> and spectral resolution of 4 cm<sup>-1</sup>. Measurements were performed on both sets of materials in different regions of the samples ( $n = 8$ ).

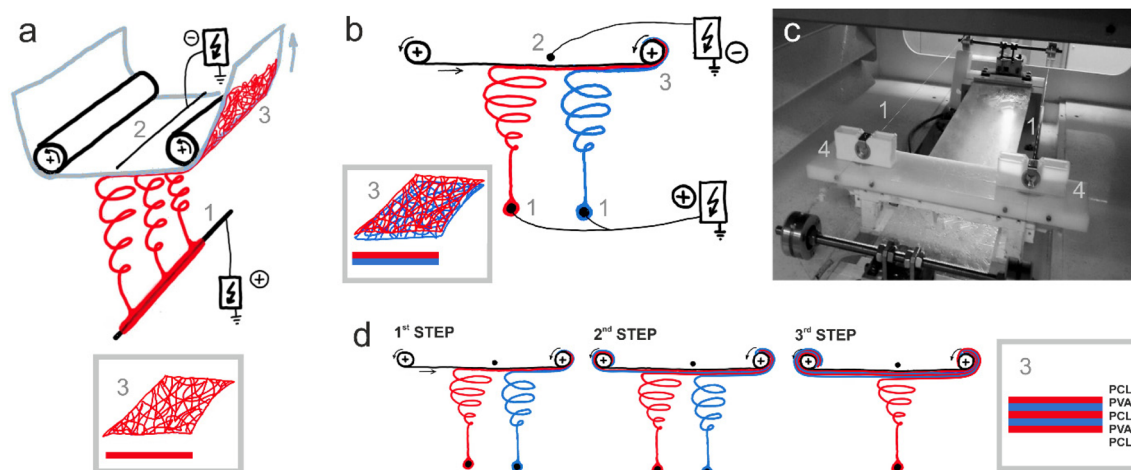


**Fig. 1** Electrospinning of the tested materials: (a) scheme of needleless direct current (DC) electrospinning from one stationary wire spinning electrode – production of a single-layer material; (b) scheme of the front view of needleless direct current electrospinning from two stationary wire spinning electrodes – production of bilayer material; (c) photographs of the inner chamber of the electrospinning device with two stationary wire spinning electrodes and (d) scheme of the three-step production of the final five-layer material combining PVA and PCL. The individual parts are: 1 – spinning electrode(s) connected to a positive source of high electric direct voltage; 2 – wire collector connected to a negative source of high electric direct voltage; 3 – the formed nanofiber layer or bilayer placed onto the ESL; 4 – movable mini-reservoirs (carriages) with polymer solutions applying solutions to stationary wires – spinning electrodes.



**Table 1** Process parameters applied during electrospinning production of nanofibrous materials

Produced material	One-layer	One-layer	Five-layer	Five-layer
<b>Process parameters</b>	<b>PCL</b>	<b>PVA</b>	<b>PCL-PVA</b>	<b>PCL-PVA + PL</b>
Spinning electrode(s) electrical voltage [kV]	50	45	50	50
Collector electrical voltage [kV]	-10	-10	-10	-10
Spinning electrode – collector distance [mm]	185	185	185	185
Orifice diameter in carriage insert [mm]	0.7	1.0	PCL 0.7	PVA 1.0
Temperature [°C]	25	25	23	24
Relative humidity [%]	17	12	25	21
Withdrawal speed [mm min <sup>-1</sup> ]	40	10	40	40

#### 2.4. Polymer distribution evaluation

The content and the distribution of the polymers in the resulting layers was evaluated using fluorescence microscopy. For this purpose, a nanofibrous material containing fluorescent dyes was prepared. The 1,1'-dioctadecyl-3,3',3'-tetramethylindocarbocyanine perchlorate (Dil; Merck, Czech Republic) was used to stain PCL, and the fluorescein 5(6)-isothiocyanate (FITC; Merck, Czech Republic) was used to stain PVA.<sup>37</sup> The PCL solution contained 16% PCL (w/w) and 0.1% Dil (w/w) in a chloroform : ethanol (8 : 2 (w/w)) solvent. The PVA solution contained 10% PVA (w/w) and 0.05 mg FITC per 100 g of solution in a water/ethanol (9 : 1 (w/w)) solvent. The materials were electrospun using two strings (see the procedure described in section 2.2.). Images of the resulting materials were captured by a fluorescence microscope (Zeiss observer Axio; Zeiss, Germany), using wavelengths  $\lambda_{\text{ex}}$  550 nm and  $\lambda_{\text{em}}$  567 nm for DiOC, and  $\lambda_{\text{ex}}$  492 nm and  $\lambda_{\text{em}}$  518 nm for FITC.

#### 2.5. Gravimetry and chromatography (GPC)

The proportion of polymers in the resulting layers was also determined using gravimetry. An amount of 0.01 g of the sample was weighed into a 10 ml vial. Then, 5 ml of the appropriate solvent – water (H<sub>2</sub>O), tetrahydrofuran (THF) and chloroform (CHCl<sub>3</sub>) was added. The samples were mixed gently and were allowed to dissolve overnight. After that, the solvent was carefully removed from the samples with a syringe to avoid damaging the nanofibrous layer. Samples in which no continuous nanofibrous layer remained were vortexed. After removing the solvent, 7 ml of new pure solvent was pipetted onto the sample and the samples were left in the solvent for at least 30 minutes with continuous careful mixing. This was repeated once more. Then, the water samples were heated in open vials in an oven at 50 °C for 1 h and were then allowed to dry for 48 h at room temperature. The THF and CHCl<sub>3</sub> samples were only allowed to dry for 48 h at room temperature. Dried samples were weighed on the same scales as before dissolution.

Samples for gel permeation chromatography (GPC) were prepared by dissolving 4 mg of material in 1 mL of water (for PVA analysis) or THF (for PCL analysis). The subsequent PVA analysis was performed according to the procedure described by Koprivova *et al.*<sup>14</sup> and the PCL analysis was performed according to the procedure described by Do Pham *et al.*<sup>38</sup> The

analysis was performed on both sets of materials and on samples from different locations of the materials ( $n = 10$ ). The resulting values are the average of these measurements, rounded to units of percent.

#### 2.6. Wettability analysis

The wettability of the PCL, PCL-PVA and PCL-PVA + PL electrospun nanofibrous materials was tested using a Krüss K121 (Krüss GmbH, Hamburg, Germany) microtensiometer.<sup>39,40</sup> A sample with a width of 30 mm and length of 40 mm was cut from the nanofibrous membrane and was placed in a holder for foils, which was then inserted into a clip with the bottom edge of the sample arranged in the horizontal position during immersion in the test liquid (distilled water). The water temperature during testing was  $21 \pm 1$  °C. The structure of the PVA nanofibrous layer alone did not allow for the testing of wettability, since a gel barrier formed during the measurements and, subsequently, the sample twisted. The wicking, *i.e.*, the weights of the distilled water that wicked into the nanofibrous materials over time, were all measured five times. The graph representing the wicked weight of distilled water into tested nanofibrous materials over time introduced different mechanisms of water adsorption and absorption in between and into the nanofibers. The total amount of water wicked into the material at the same time (in this case 250 s) can be compared. The spontaneous wicking of porous materials, including textiles and nanofibrous layers, can be described *via* the application of the Washburn equation. The results, given in the form of the average squared mass gain over time from the beginning of the wicking process, represented the wicking rate *via* the direction of the regression curve.

#### 2.7. Hemocompatibility

The hemocompatibility of the prepared membranes, *i.e.* hemolysis, thrombogenicity and coagulation, was tested using the methodology described in our previous work.<sup>41</sup> For testing the hemolysis, diluted anticoagulated blood was used (4 ml of blood was diluted in 5 ml in PBS pH 7.4). Samples (1 cm<sup>2</sup>,  $n = 5$ ) were placed into 10 ml of PBS (pH 7.4), and after 30 min incubation at 37 °C, 200  $\mu$ l of prepared blood solution was added. After 1 hour of incubation at 37 °C, the tubes were centrifuged (100g for 20 min) and the hemoglobin concentration in the supernatant was measured at 570 nm using a spectro-



photometer (TECAN spectrophotometer, Austria). Distilled water was used as the positive control and PBS without material was used as the negative control. The degree of hemolysis (%) was recalculated using the following formula, where  $A_{\text{sample}}$  is the average absorbance of the test sample group,  $A_{\text{neg}}$  is the absorbance of the negative control group and  $A_{\text{pos}}$  is the absorbance of the positive control group:

$$\% \text{hemolysis} = [(A_{\text{sample}} - A_{\text{neg}}) / (A_{\text{pos}} - A_{\text{neg}})] \times 100. \quad (1)$$

Thrombogenicity was measured using a freshly-prepared (24 hours after donation, gently agitated at 20–24 °C) platelet-rich solution (PRS) containing  $688 \times 10^9$  platelets per L. The 1 cm<sup>2</sup> sterilized samples ( $n = 10$ ) were placed into a 48-well plate and were incubated in 1 ml of PRS at 37 °C for 2 hours. Samples incubated in pure Intersol solution were used as a negative control, and PRS incubated in the well plate was used as a positive control. To measure the viability of the platelets, we used a CCK-8 colorimetric assay kit. The samples were incubated in PRS for 2 hours, and then they were incubated in a CCK-8 solution, previously diluted in an InterSol solution at 1 : 9 (v/v) for 2 hours at 37 °C. The concentration of the forming product was measured using a spectrophotometer at 450 nm.

The effect of the samples on coagulation was evaluated by measuring the prothrombin time test (PT) and the activated partial thromboplastin time test (aPTT) using platelet pure plasma (PPP) obtained from the regional hospital in Liberec (Czech Republic). Samples (1 cm<sup>2</sup>,  $n = 5$ ) were placed into 0.5 ml of PPP in a low-binding protein microtube (Eppendorf, Germany) and were incubated for 45 min at 37 °C. As a negative control, 0.5 ml of PPP was incubated in a tube without any material. After incubation, the materials were removed from the test tubes and the PT and aPTT clotting times of the remaining plasma were measured using a BCS XP automatic analyser (Siemens) according to the instructions for the device.

## 2.8. Cell culture and monocultures

HaCaT human keratinocytes (CLS Cell Lines Service GmbH) were cultured in Dulbecco's modified Eagle's medium (DMEM; ThermoFisher Scientific) supplemented with 10% fetal bovine serum (FBS; ThermoFisher Scientific) under standard conditions (humidified atmosphere, 37 °C and 5% CO<sub>2</sub>). Normal human dermal fibroblasts from neonatal foreskin (NHDFs; Lonza) were cultured in DMEM with 10% of FBS. Early passages of NHDFs (passages 2–4) were used for the experiments. Primary human saphenous vein endothelial cells (HSVECs; Provitro) were cultured in Endothelial Cell Growth Medium 2 (EGM-2) with supplements (PromoCell GmbH, Germany, Cat. No. C-22111). For the experiments, passages 3 and 4 were used. For monocultures of HaCaT cells and NHDFs, the membranes were cut into pieces of 1 cm<sup>2</sup> area and were placed in a 24-well plate. Both cell types were seeded at a density of 20 000 cells per well and were cultured over time. For monocultures of HSVEC, 20 000 cells were seeded per well in 1 mL of medium in a 24-well culture plate (Cellvis, USA). Then, the membranes were placed into each well on HSVECs.

## 2.9. Co-culture system

A co-culture system was developed to allow the growth of keratinocytes and fibroblasts on both sides of the membranes. A 3D model of the insert for seeding the membrane from both sides (Fig. S1†) was created in FreeCAD software (The FreeCAD Team). This model was then exported to the additive manufacturing file (amf) format and was transferred to the PrusaSlicer software (Prusa Research, Czech Republic). The 3D model of the insert was multiplied in PrusaSlicer and the Gcode file for 3D printing was then exported from the PrusaSlicer and downloaded to the 3D printer. The insert was printed on the Original Prusa i3 MK3S 3D printer (Prusa Research, Czech Republic) from colorless polylactic acid (PLA) filament PLA Extrafill Crystal Clear (Fillamentum, Czech Republic, 1.75 mm diameter, working temperature: 210–230 °C). The printer was equipped with a 0.4 mm hole nozzle, and the thickness of a single printed layer was set to 0.15 mm. For co-culture experiments of the three cell types, a density of 20 000 NHDF cells per well was seeded on one side of the membranes and, after 1 hour required for cell adhesion, the membranes were placed upside down in a fresh cell culture plate. Then, HaCaT cells were seeded at a density of 50 000 cells per well on the opposite side of the membranes. In parallel, 20 000 cell HSVECs were seeded in a 24-well plate. After 3 hours to allow the adhesion of the HaCaT cells and HSVECs, the membranes containing both NHDFs and HaCaT cells were placed into well-plates pre-seeded with HSVECs (Fig. 2). Cells were cultured for 7 days in DMEM with 10% FBS and EGM-2 medium with standard supplements at a ratio of 1 : 1. The cell culture medium was partially replaced each 2–3 days. In addition, co-cultures of HaCaT and NHDFs growing on nanofibrous membranes were performed without the presence of endothelial cells. For these experiments, only DMEM with 10% of FBS was used as a culture medium.

## 2.10. Metabolic activity/cell proliferation

The metabolic activity was determined by a CellTiter 96@ Aqueous One Solution Cell Proliferation Assay (MTS, Promega

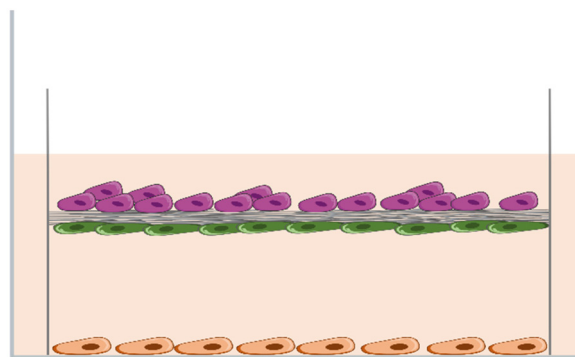


Fig. 2 Schematic illustration of the co-culture system used in the experiments with the HaCaT keratinocytes (top cells), the normal human dermal fibroblasts (middle cells), and the human saphenous vein endothelial cells (bottom cells).



Corporation). The nanofibrous membranes with cells were transferred to fresh 24-well plates for MTS analysis for each time point tested. The samples were incubated with 500  $\mu\text{l}$  of phenol red-free DMEM supplemented with 10% of FBS and 100  $\mu\text{l}$  of MTS for 1 hour under standard conditions. The absorbance was measured using a VersaMax ELISA Microplate Reader spectrophotometer (Molecular Devices Corporation) at a wavelength of 490 nm and was normalized per well.

### 2.11. Cytoskeleton visualization

Following the MTS assay, the cells were rinsed with phosphate-buffered saline (PBS) and were fixed with 4% paraformaldehyde in PBS for 20 min. The initial cell adhesion and cell morphology were analyzed by staining the cells with phalloidin after 1 day in culture. In addition, cells that had been cultured for 7 days were stained with phalloidin. The samples were incubated with Atto 488-conjugated phalloidin (1 : 500; Sigma-Aldrich) and were counterstained with Hoechst 33258 (5  $\mu\text{g mL}^{-1}$  in PBS, Sigma-Aldrich) for 20 min at room temperature (RT). Images of the adherent cells were captured under an IX-50 microscope equipped with a DP 70 digital camera (both from Olympus) and under a Dragonfly 503 spinning disk confocal microscope equipped with a Zyla 4.2 PLUS sCMOS camera (Andor, Belfast, UK).

### 2.12. Immunofluorescence staining of specific cell markers

Immunodetection of specific markers was performed on keratinocytes, fibroblasts and endothelial cells. The cells were fixed in 4% paraformaldehyde in PBS for 20 min at RT, were permeabilized with 1% of BSA in PBS containing 0.1% Triton X-100 for 20 min, and were treated with 1% of Tween for 20 min at RT. For the staining of cytokeratin 14 intermediate filaments in the keratinocytes, samples were incubated with a mouse monoclonal anti-cytokeratin 14 primary antibody (1 : 400; Abcam, Cambridge, UK, Cat. No. ab7800) overnight at 4 °C. After being rinsed twice with PBS, the samples were incubated with a solution of Alexa Fluor 546-conjugated goat anti-mouse secondary antibody (1 : 400; Thermo Fisher Scientific, Waltham, MA, USA; Cat. No. A11003) with Hoechst 33258 dye (5  $\mu\text{g mL}^{-1}$ , for the staining of the cell nuclei) for 2 hours at RT. The collagen synthesis of the fibroblasts was evaluated *via* the immunodetection of type I collagen. The samples were then incubated with a rabbit monoclonal anti-collagen type 1 primary antibody (1 : 400; Abcam, Cambridge, UK), overnight at 4 °C, were washed in PBS, and were subsequently incubated with an Alexa Fluor 488-conjugated goat anti-rabbit secondary antibody (1 : 400; Thermo Fisher Scientific, Waltham, MA, USA; Cat. No. A11070) for 1 h together with a Hoechst 33258 dye (5  $\mu\text{g mL}^{-1}$ ) for staining the cell nuclei. Then, images were captured using a Dragonfly 503 spinning disk confocal microscope equipped with a Zyla 4.2 PLUS sCMOS camera. The area covered by HaCaT cells on nanofibrous membranes and the fluorescent intensity of type I collagen synthesized by NHDFs were quantified using ImageJ software. The phenotypic maturation of the HSVECs was analyzed by immunostaining the von Willebrand factor. The samples were incubated with a

rabbit anti-von Willebrand factor primary antibody (1 : 400, Sigma-Aldrich, Merck, Darmstadt, Germany, Cat. No. F3520) overnight at 4 °C. Then, the samples were rinsed twice with PBS and were incubated with an Alexa Fluor 488-conjugated goat anti-rabbit secondary antibody (1 : 400, Thermo Fisher Scientific, Waltham, MA, USA; Cat. No., Cat. No. A11070). Images of endothelial cells were captured under an IX-71 microscope equipped with a DP 70 digital camera (both from Olympus, Tokyo, Japan). The cell numbers were determined by counting the cell nuclei using ImageJ software. At least 12 randomly selected microphotographs were evaluated for each analysis.

### 2.13. Scratch-wound assay

Scratch wounds were created in confluent monolayers of NHDFs by using a sterile 100  $\mu\text{l}$  pipette tip. A total amount of 100 000 cells were seeded on a 24-well plate. After 48 hours, a confluent monolayer of cells was obtained and a scratch wound was created in each well. After washing with PBS twice and after adding new media, images of the wounds were captured under an IX-71 microscope equipped with a DP 70 digital camera (both from Olympus, Tokyo, Japan). Then, PCL-PVA + PL and PCL-PVA membranes were placed into the wells. Cell migration into the wound space was analyzed after 8 hours by measuring the clear space between the wound edges with image analysis using ImageJ software. Time zero width was used as an initial wound measurement. Results are shown as a percentage of wound closure (percentage reduction of clear space).

### 2.14. Endothelial transmigration assay

The migration of HSVECs through 8  $\mu\text{m}$ -diameter pores was analyzed using FluoroBlok cell culture inserts (Corning, New York, NY, USA). The membranes (PCL-PVA + PL and PCL-PVA) were placed in a 24-well culture plate with a low-supplemented EGM-2 medium. Then, cell culture inserts were placed in each well and 20 000 HSVECs were seeded in the inserts. After 4 h, the inserts were washed with PBS and were fixed with 4% paraformaldehyde in PBS for 15 min at RT. The cells were then stained with a solution of Texas Red C<sub>2</sub>-maleimide cell membrane dye (1.7  $\mu\text{g mL}^{-1}$  in PBS, ThermoFisher Scientific, Waltham, MA, USA) and Hoechst 33258 nuclear dye (5  $\mu\text{g mL}^{-1}$  of PBS) for 45 min at RT. Images of the cells that migrated through the insert pores were captured under an Olympus IX-71 epifluorescence microscope equipped with a DP80 digital camera (both from Olympus, Tokyo, Japan).

### 2.15. Statistical analysis

The quantitative data were presented as the mean with the standard error of the mean. Statistical comparisons were performed using the one-way analysis of variance (ANOVA) with the Tukey multiple comparisons test. Non-normally distributed numerical data are expressed as the median and interquartile range (IQR), and statistical comparisons were performed using nonparametric analysis followed by the Kruskal–Wallis test for multiple comparisons. In all cases, the analysis was



performed using GraphPad Prism 5 (GraphPad Software, San Diego, CA, USA). A  $p$ -value of  $p \leq 0.05$  was considered statistically significant.

### 3. Results and discussion

#### 3.1. Preparation and characterization of nanofibrous membranes

The materials were prepared by DC electrospinning under controlled conditions. The spinning process for mixed materials is clearly influenced by the presence of the second spinning system. This factor significantly affects the production rate of both polymers, as well as the morphology of the resulting materials. The materials prepared by DC electrospinning were further analyzed in terms of morphology, the content of polymer types and incorporated proteins, and wettability.

**3.1.1. Morphology of nanofibrous membranes.** The morphology of the materials was evaluated from two sets of prepared materials. The diameters of the fibers in the pure PCL, and in the multilayered membranes PCL-PVA and PCL-PVA + PL were quantified (Fig. 3). In addition, the diameters of the pure PVA and PVA + PL were quantified for comparison with the multilayers (Fig. S2†). The pure materials showed higher values than for the multilayers. The largest diameter of the fibers was measured for PCL materials ( $420 \pm 500$  nm, Fig. 3A), where there is also a wider distribution of fiber diameters (expressed by the standard deviation). Large average fiber diameters were also measured for PVA ( $380 \pm 150$  nm) and PVA + PL ( $390 \pm 150$  nm). For PVA + PL, the fiber diameter is unaffected by the presence of incorporated proteins, corres-

ponding to previously published data by Koprivova *et al.*<sup>14</sup> Composite materials have significantly smaller fiber diameters, both for PCL-PVA ( $300 \pm 130$  nm) and for PCL-PVA + PL ( $310 \pm 160$  nm) (Fig. 3B and C); the distribution of the fiber diameter is comparable to pure PVA materials. Given that the upper side of the composite material is always formed mainly by PCL fibers (see scheme in Fig. 1), it can be assumed that this change in the diameters of the PCL is probably caused by the presence of the second spinning system during the spinning process. The simultaneous spinning of PVA will affect both the local humidity and the distribution of the electric field.<sup>26</sup> The result is a significantly larger proportion of fine fibers and a reduced presence of thick fibers, which is also evident in the scanning electron microscope (SEM) images (Fig. 3).

For materials that were further tested for biocompatibility, the surface density was analyzed (Table 2). The surface density of the materials was similar and ranged between  $45\text{--}49$   $\text{g m}^{-2}$ .

**3.1.2. Composition analysis of nanofibrous membranes.** The chemical composition of the prepared materials and the homogeneity of their distribution within the prepared layers was further evaluated by attenuated total reflection Fourier

**Table 2** Morphology of the nanofibrous membranes

	PCL	PCL-PVA	PCL-PVA + PL
Mean of fiber diameter (nm)	419	302	306
Std. deviation (nm)	500	131	158
Lower 95% CI of mean (nm)	368	289	290
Upper 95% CI of mean (nm)	471	316	323
Surface density ( $\text{g m}^{-2}$ )	49.06	45.19	47.81
Std. deviation ( $\text{g m}^{-2}$ )	5.98	4.98	1.85

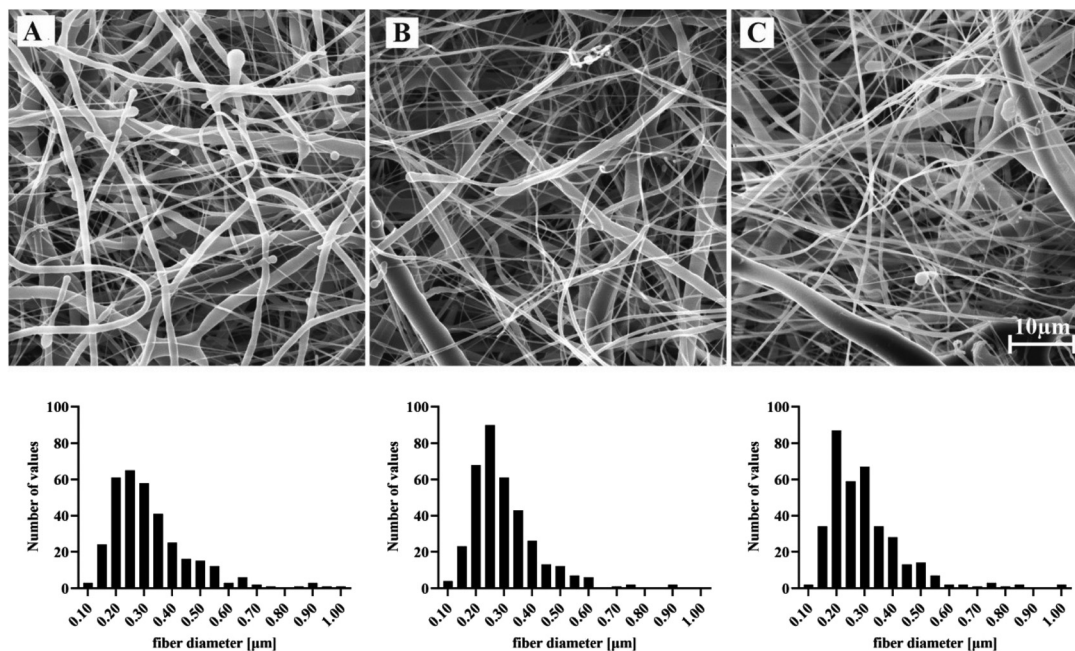


**Fig. 3** Representative SEM micrographs and the corresponding fiber diameter distributions ( $n = 360$ ) of electrospun materials: PCL (A), PCL-PVA (B) and PCL-PVA + PL (C). Scale bar  $10 \mu\text{m}$ .



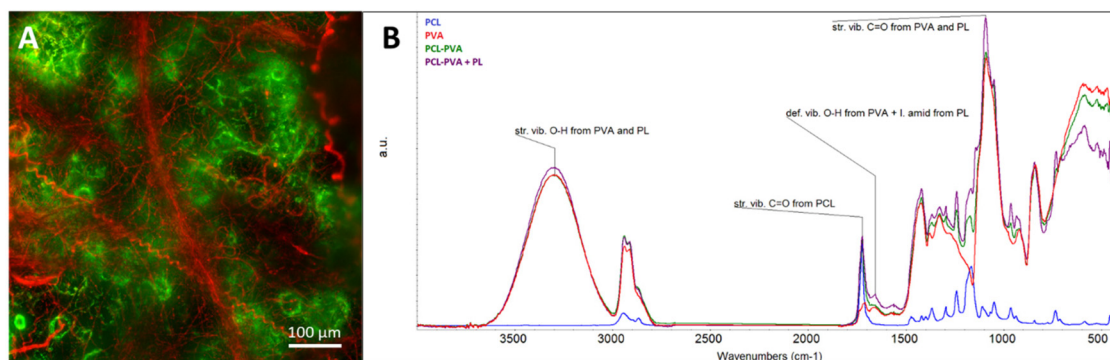


**Fig. 4** (A) Fluorescence microscopy of a nanofibrous layer combining fluorescently labeled PCL fibers (in red, staining with Dil) and PVA fibers (in green, staining with FITC), scale bar = 100  $\mu\text{m}$ . (B) ATR-FTIR analysis of spectra from nanofibrous materials: PVA, PCL, PCL-PVA and PCL-PVA + PL.

transform infrared spectroscopy (ATR-FTIR) analysis, by fluorescence microscopy evaluation, and by gravimetry.

The resulting spectra obtained by FTIR analysis of the materials (Fig. 4B) confirmed the presence of both polymers (PCL and PVA) in the case of the PCL-PVA layer, and in the case of the PCL-PVA + PL layer, also the presence of incorporated proteins. The PCL spectrum evinced a strong peak at  $1724\text{ cm}^{-1}$  (C=O bonding). The PVA spectrum contained characteristic peaks at  $3299\text{ cm}^{-1}$  (O-H stretching), at  $2917\text{ cm}^{-1}$  (C-H stretching from  $-\text{CH}_2-$ ),  $1427\text{ cm}^{-1}$  (C-H deformation) and at  $1085\text{ cm}^{-1}$  (C-O stretching).<sup>42</sup> Amide bonds within the protein absorbed radiation in multiple regions, including a strong band at  $1600\text{--}1690\text{ cm}^{-1}$ .<sup>43</sup>

The presence and the distribution of fibers in the composite nanofibrous material were analyzed in the materials containing fluorescent dyes (FITC in the case of PVA, and Dil in the case of PCL). The evaluation (Fig. 4A) confirmed the presence of both types of fibers in the resulting composite layer; however, the distribution was not completely uniform. Some areas contained more PVA or PCL fibers, which can be explained by the mutual repulsion of hydrophilic PVA and hydrophobic PCL during the electrospinning process. In addition, the spinnability of both polymeric solutions together during multi-jet electrospinning was probably permitted by the configuration, in which the simultaneously spun PVA aqueous solution affected both the local humidity and the distribution of the electric field.<sup>26</sup>

The quantification of the individual polymers in the prepared composite materials was carried out by gravimetry, using the different solubility of the individual components – the PVA was dissolved in water and then the remaining PCL component was weighed, or the PCL was dissolved in THF and  $\text{CHCl}_3$  with subsequent weighing of the remaining PVA component of the material. The PVA content in the PCL-PVA material was  $5 \pm 2\%$  (w/w), and the PVA content in the PCL-PVA + PL material was  $7 \pm 2\%$  (w/w). Quantification performed using chromatography showed that the PVA content in the PCL-PVA material was  $6 \pm 5\%$  (w/w), and the PVA content in the PCL-PVA + PL material was  $5 \pm 4\%$  (w/w). The measured values have a large variance, which is probably due to the repulsion

of hydrophilic PVA and hydrophobic PCL during the production of the material, or due to the imperfect dissolution of the materials in two different solvent systems during the subsequent analysis. For the reasons stated above, we take the results more as indicative, proving the presence of PVA in composite materials in amounts between 1–9% (w/w). The results indicate that the inhomogeneity of the material is significant, but it has a defined lower and upper bound.

The presence of proteins in the PCL-PVA + PL material was confirmed by the FTIR method (Fig. 4B). However, the exact protein content was not evaluated because the used methods were below the detection limits. Based on an analysis of the PVA content in the composite PCL-PVA + PL material and the protein content in the pure PVA-PL material (protein loading efficiency 0.64%), the theoretical protein content in the composite material is between 0.006–0.05% (w/w).<sup>14</sup>

**3.1.3. Wettability of the prepared materials.** The PCL, PCL-PVA and PCL-PVA + PL differed in their wettability in distilled water. The wicking included spontaneous water penetration between fibers, and in the case of PVA content, also absorption into fibers. The penetration into the PCL nanofibers was significantly lower than the penetration into the PCL-PVA and PCL-PVA + PL materials (Fig. 5A). The beginning of penetration differed for PCL-PVA and PCL-PVA + PL, but for relatively long time intervals, their total amount of wicked water was similar. The rate of penetration into porous materials described by mean squared weight *versus* time had a linear trend at the beginning of penetration (Fig. 5B), but also differed significantly for the tested materials. The penetration into PCL-PVA was more than two times faster than into PCL and, in the case of PCL-PVA + PL, it was more than fifteen times faster than into PCL. The water distribution in the tested samples also showed a difference between their behavior connected with wettability by water (Fig. S3†). The test demonstrated that the best wettability was observed on the PCL-PVA + PL nanofibrous membranes.

### 3.2. Hemocompatibility of nanofibrous membranes

When materials are intended to be used as wound dressings, it is advisable to find out whether they are thrombogenic (risk





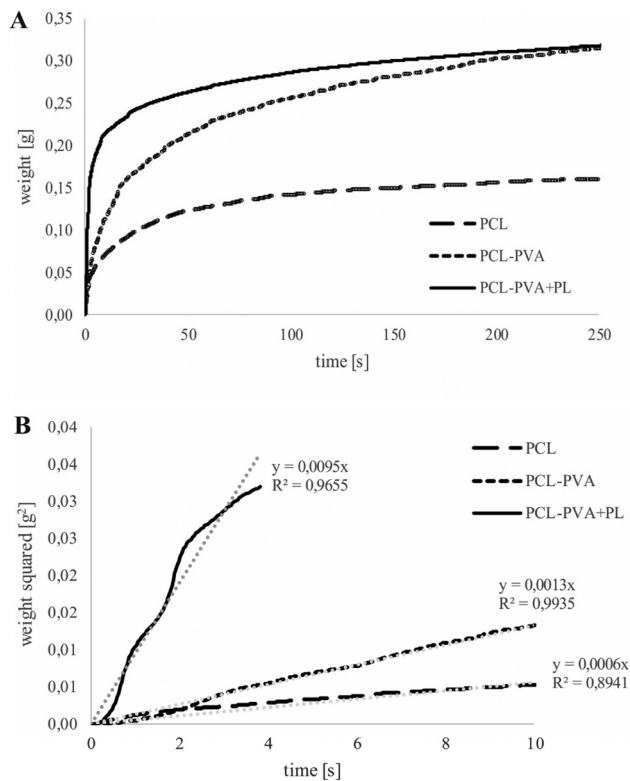


**Fig. 5** Mean (A) and mean squared (B) weight of water wicked into the PCL, PCL-PVA and PCL-PVA + PL electrospun nanofibrous materials in time. The mean squared weights at the beginning of penetration are connected by linear trend equations and squared regression coefficients.

of thrombus formation due to the application of the materials), whether blood coagulation is affected (reduction in coagulation speed), and whether the membrane of red blood cells is disrupted. The prepared membranes were therefore evaluated in terms of their hemocompatibility including thrombogenicity, hemolysis and coagulation tests.

The contact between platelets and materials could accelerate the activation of the platelets. The degree of activation can be monitored by means of a cell viability measurement test. The interaction between materials and native platelets was assessed by measuring the platelet viability, which corresponds to the rate of platelet activation.<sup>41</sup> The results (Fig. 6 and Fig. S4†) showed that all tested membranes influenced the platelet activation when compared to the control (tissue culture plastic). The results also showed that the chemical composition – the presence of PVA and/or PL – does not affect platelet activation. From this point of view, this study confirms the previous finding that platelet activation is accelerated mainly because of the nanofibrous structure of the material.<sup>41</sup> The morphological similarity between nanofibrous materials and the native extracellular matrix can therefore be a disadvantage of these materials in some applications, and the risk of increased activation of platelets should be taken into consideration. On the other hand, accelerated activation of platelets can also promote the wound-healing process.

Some materials can damage the erythrocyte membrane (mainly *via* denaturation of membrane proteins), causing hemoglobin to be released into the environment. This test is one of those used to assess nanomaterials and biomaterials toxicity *in vitro*.<sup>44,45</sup> Analysis of erythrocyte hemolysis after the interaction of materials with diluted whole human blood is based on spectrophotometric detection of hemoglobin at 570 nm (Fig. 6B and C). The highest concentration of released hemoglobin was caused by distilled water, and the lowest concentration was caused by phosphate-buffered saline (PBS) without added material. Similar values were observed for the three membrane types. After recalculation, the degree of hydrolysis of the positive control (PC; distilled water) was  $100 \pm 1.5\%$ . For the negative control (NC; PBS) was  $0 \pm 0.8\%$ ; for PCL the degree of hydrolysis was  $1.8 \pm 2.8\%$ ; for PCL-PVA the value was  $1.1 \pm 1.7\%$ ; and for PCL-PVA + PL the value was  $2.5 \pm 3.2\%$ . According to the ISO 10993-4:2002 standard and ASTM F756-00(2000), the degree of hemolysis must be  $<5\%$ . Based on these results, it can be said that none of the materials is hemolytic.

Contact of the material with blood plasma may affect the rate of coagulation; in the case of materials with an anti-coagulant effect, the coagulation time is prolonged. As part of the coagulation analysis, the PT test (prothrombin time, also referred to as the QUICK test, external coagulation pathway monitoring) and the aPTT test (activated partial thromboplastin time, internal coagulation pathway monitoring) were performed. The result of the PT test (Fig. 6D) shows that PCL and PCL-PVA + PL nanofibrous materials increase the average PT coagulation time compared to the control (clinical plasma without the addition of material). In the case of the aPTT test (Fig. 6E), no significant prolongation is observed. However, a clinically significant difference in coagulation times is assessed as a greater than 20% difference from the control value,<sup>46</sup> which does not occur in this case, and the materials have no clinically significant anticoagulant effect.

### 3.3. Cytocompatibility of nanofibrous membranes

The cell adhesion and cytoskeleton organization of the cells grown on the membranes were evaluated after 24 hours in culture. The results indicated that human keratinocytes (HaCaT cells) were able to adhere on all samples, *i.e.*, PCL-PVA + PL, PCL-PVA and PCL nanofibrous membranes. The cells showed a rounded shape and created small island-like clusters, which is the morphology usually observed in keratinocytes after 24 h of culturing (Fig. 7A). Normal human dermal fibroblasts (NHDFs) were also able to adhere and spread on the three nanofibrous membranes analyzed. The cell morphology of the fibroblasts showed no clear differences among the samples. In all cases, the morphology was polygonal or spindle-shaped, with a small number of rounded shape cells (Fig. 7A). Keratinocytes and fibroblasts are anchorage-dependent cells, which means that they need to adhere to a substrate to grow. PCL has been extensively investigated for tissue engineering applications due to its interesting properties and biocompatibility.<sup>47</sup> However, there is poor cell adhesion on some



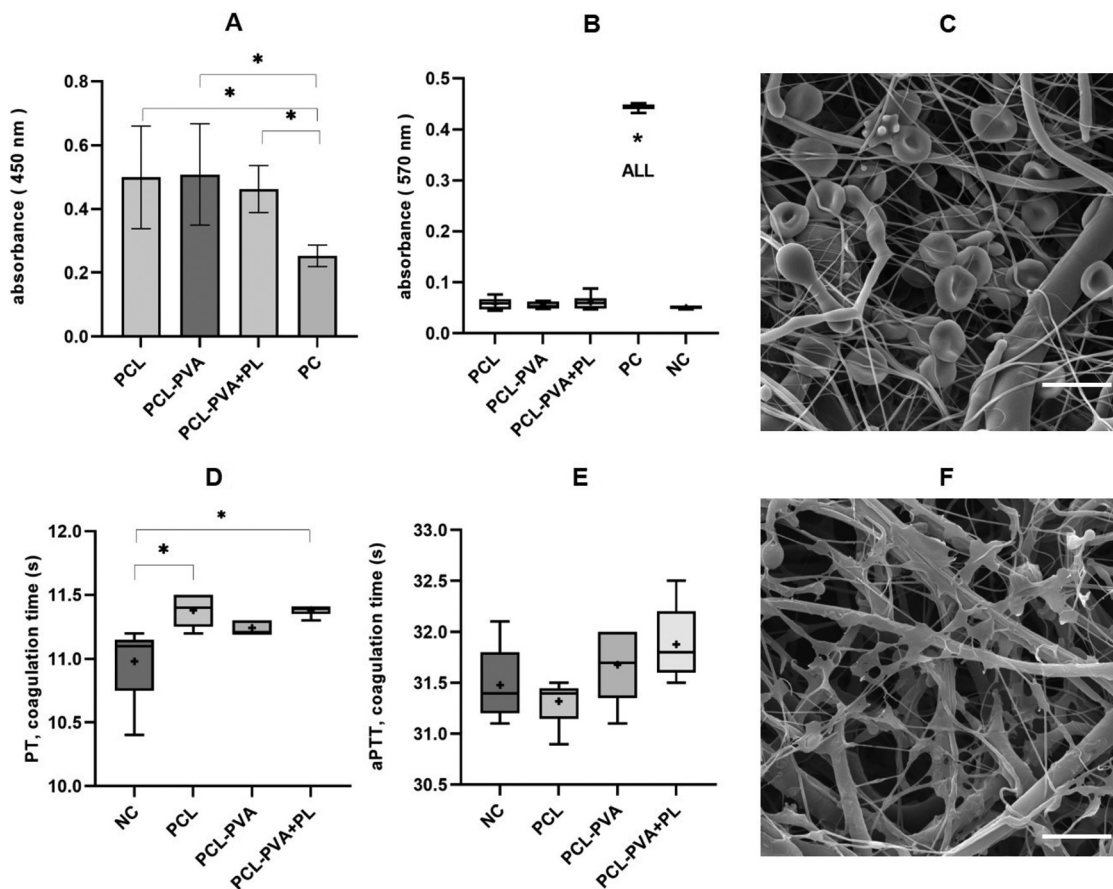


**Fig. 6** Hemocompatibility of DC electrospinning prepared multilayers. (A) A graph representing a material thrombogenicity test (*i.e.*, viability of platelets that adhered from platelet-rich solution onto the material, PC – the well plate bottom). (B) A graph of the hemolysis test (*i.e.*, hemoglobin released from damaged blood cells upon contact of the material with diluted anticoagulated blood, PC – distilled water, NC – without material). (C) SEM picture of PCL-PVA material after incubation with diluted whole blood (scale bar 10  $\mu$ m). D, E: graphs representing coagulation tests, *i.e.* the stimulation of coagulation cascade after the contact of the materials with platelet pure plasma; (D) prothrombin time (PT; NC – plasma without material), and (E) activated partial thromboplastin time (aPTT; NC – plasma without material). (F) SEM picture of PCL-PVA + PL material after 2 h incubation with platelets (scale bar 10  $\mu$ m). The asterisks indicate significant differences between samples ( $p < 0.05$ ).

types of PCL surfaces. PCL is therefore widely used in combination with other polymers for wound repair. Our results for initial cell attachment, spreading and morphology showed no clear differences among the samples, which indicates that the PCL, PCL-PVA and PCL-PVA + PL nanofibrous membranes allowed cell adhesion. However, the wettability of PCL was lower than for PCL-PVA nanofibrous membranes with and without PL. In this regard, the developed multilayered nanofibrous membranes provided suitable growth support for skin cells.

The metabolic activity of the HaCaT cells (Fig. 7B) and NHDF (Fig. 7C), cultured on the membranes for days 1, 3 and 7 was quantified. The cells proliferated on both tested membranes, without any signs of cytotoxic or cytostatic effects. On days 1 and 3 after seeding, the metabolic activity of the HaCaT cells and NHDFs showed no significant differences between PCL, PCL-PVA and PCL-PVA + PL nanofibrous membranes. On day 7, similar metabolic activity was observed for HaCaT cells. However, the metabolic activity of NHDF cultured for 7 days was observed to be higher on membranes containing PL than

on membranes without PL and PCL. Previously, we had demonstrated that PVA nanomats containing PL, immersed in the culture medium, enhanced the metabolic activity of 3T3 fibroblasts on day 7, and the metabolic activity of HaCaT cells on day 1, when these cells were cultured in DMEM medium with 2% of FS.<sup>35</sup> PL contains a mixture of cytokines, growth factors and other bioactive molecules, which can influence the behavior of keratinocytes and fibroblasts. Indeed, PL has been demonstrated that it can accelerate the proliferation of fibroblasts, keratinocytes and endothelial cells.

On day 7 following cell seeding on the membranes, the HaCaT cells were found to be positive for cytokeratin 14 (Fig. 8A–C). Basal cytokeratin 14 was present as an intermediate filament of all cells that were observed. The cells grew as big islands that almost reached a monolayer in several parts of the nanofibrous membranes. A similar number of cells was observed for the PCL-PVA + PL, PCL-PVA, and PCL membranes, which is in accordance with the metabolic activity results previously described. In addition, NHDFs growing on the other



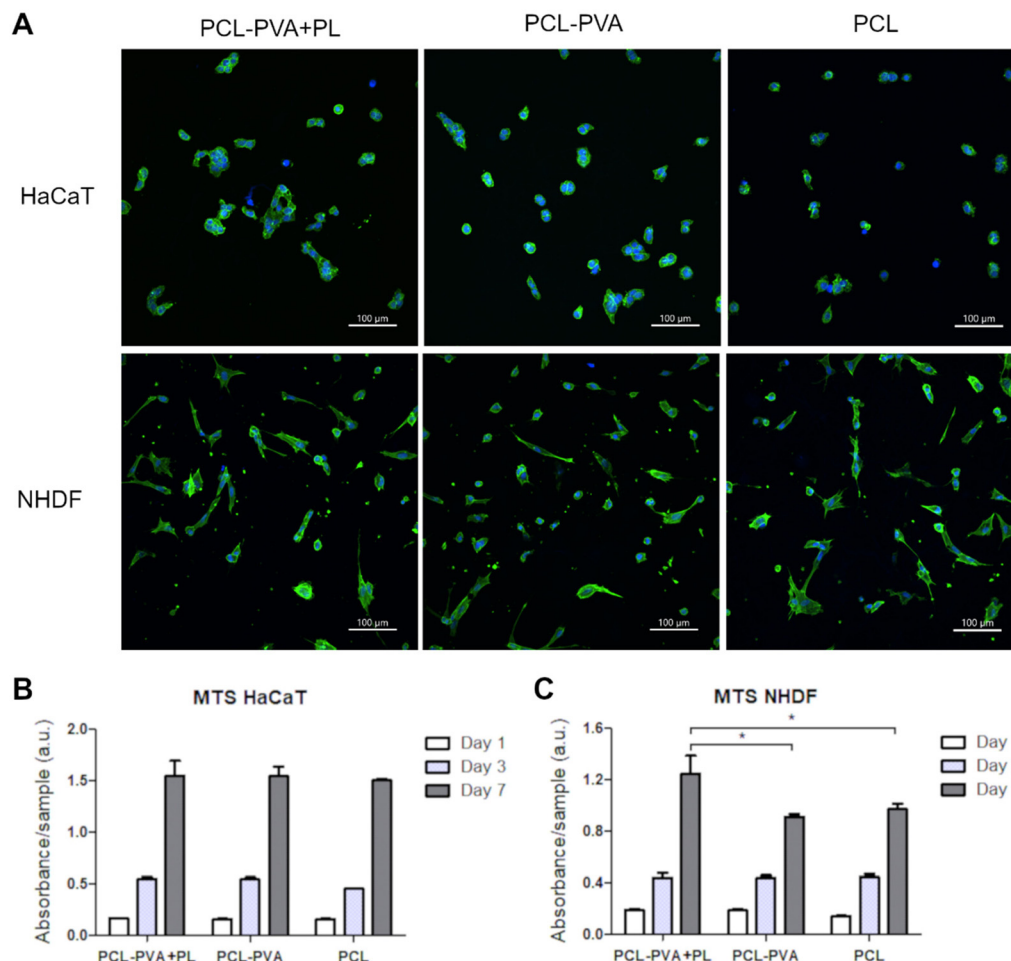


**Fig. 7** Adhesion of HaCaT cells and NHDFs on PCL-PVA + PL, PCL-PVA and PCL nanofibrous membranes on day 1 after seeding (A). Images of the cells stained with phalloidin-Atto488 (green) and counterstained with Hoechst 33258 (blue) captured using an Andor Dragonfly 503 spinning disk confocal microscope equipped with a Zyla 4.2 PLUS sCMOS camera. The metabolic activity of HaCaT cells (B) and NHDFs (C) on the PCL-PVA + PL, PCL-PVA and PCL nanofibrous membranes in monocultures was evaluated within 7 days after cultivation. The asterisks indicate significant differences between samples for each cell type and time point ( $p < 0.05$ ).

side of the membrane were visualized by immunofluorescence staining of type I collagen. Collagen was present on all membranes tested, although a higher number of cells and collagen synthesis was observed on PCL-PVA + PL compared to both PCL-PVA and PCL membranes (Fig. 8D–F).

The PL used to prepare the PVA + PL solution contained several growth factors that play an important role in skin regeneration, *i.e.* PDGF, bFGF, and VEGF. The concentration of each growth factor present in the PL showed values in the range of  $\text{ng mL}^{-1}$  for PDGF and  $\text{pg mL}^{-1}$  for the FGF and VEGF.<sup>36</sup> However, the theoretical protein content in the PCL-PVA + PL membranes was calculated to be between 0.006–0.05% (w/w). Thus, the specific concentration of each growth factor is under the detection limit. The results for HaCaT proliferation and distribution showed no significant differences among the samples, although differences in proliferation were observed for the NHDF cells. PL enhanced the proliferation of fibroblasts, despite the low concentration of growth factors. A more pronounced response of fibroblasts

than of keratinocytes to the PL released from the membranes is in accordance with previous studies on the bioactivity of PVA + PL nanomats on skin cells, *i.e.* 3T3 fibroblasts, HaCaT cells and human saphenous vein endothelial cells (HSVECs).<sup>35</sup>

### 3.4. Bioactive effect of nanofibrous membranes on co-cultured keratinocytes, fibroblasts, and endothelial cells

Three different cell types with an important role in the wound healing process were co-cultured to analyze their paracrine effect when cultured with nanofibrous membranes.

Firstly, HaCaT cells and NHDFs were co-cultured without the addition of HSVECs. The nanofibrous membranes allowed a co-culture of keratinocytes and fibroblasts on the opposite sides of the membrane. The membrane was therefore used as a barrier to segregate each cell type. In addition, the nanofibrous membrane was used as an artificial basement membrane, which constitutes the anchorage of the epithelium and the connective tissue in skin tissue. Under *in vitro* conditions, the membranes created a physical barrier to avoid direct contact



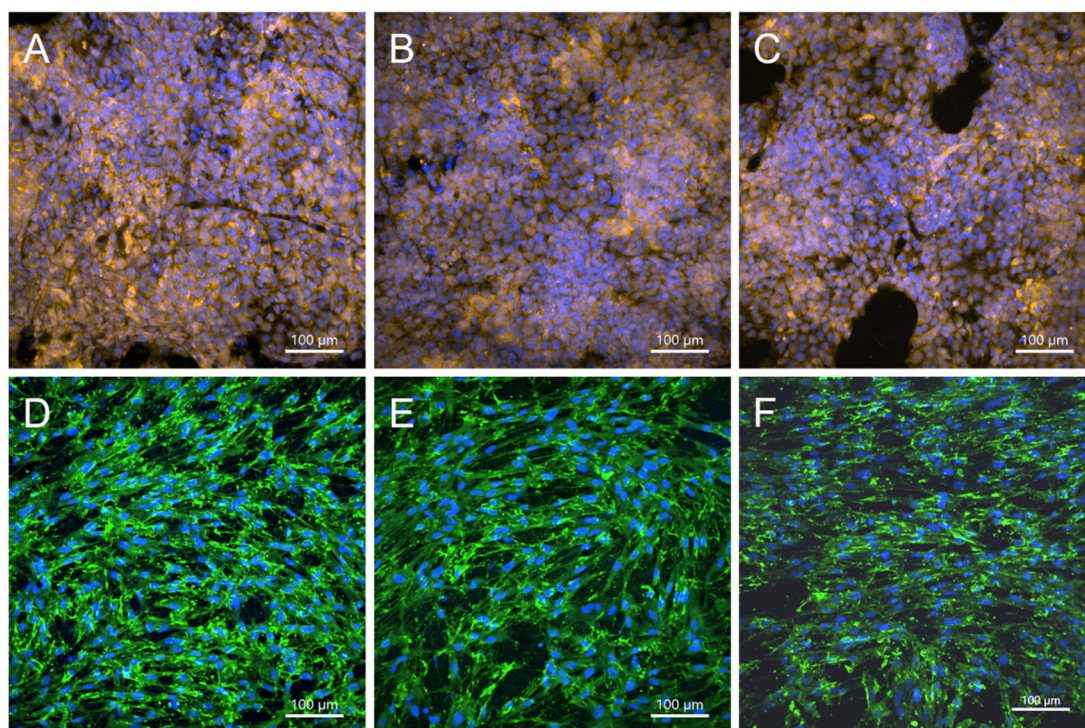


**Fig. 8** Cytokeratin 14 (gold) of HaCaT cells (A–C) and type I collagen (green) of NHDFs (D and F) that grew on PCL-PVA + PL (A and D), PCL-PVA (B and E), and PCL (C and F) nanofibrous membranes for 7 days. Cells were also stained by Hoechst (blue) and images were captured using an Andor Dragonfly 503 – spinning disk confocal microscope equipped with a Zyla 4.2 PLUS sCMOS camera.

between the two cell types and the potential overgrowth of one of them. However, the nanofibrous membranes allowed molecular exchange by sharing the cell culture medium and all the bioactive compounds secreted by the cells.

The morphology and the cytoskeleton organization of the cells co-cultured on the membranes were analyzed by actin stress fiber staining on day 7 after cell seeding (Fig. S5†). Images showed that HaCaT cells were able to proliferate on both PCL-PVA and PCL-PVA + PL membranes, and the morphology was also similar on both membranes. The fibroblasts proliferated on the membranes and were oriented in parallel. Both cell types created a monolayer on membranes containing PL, but several void spaces were observed on samples without PL. The results were in agreement with the previous results obtained on monocultures. The PL enhanced the proliferation of fibroblasts in monocultures, and it also enhanced the proliferation of keratinocytes in co-cultures. We hypothesize that the presence of fibroblasts could have a positive influence on the proliferation of keratinocytes. It has previously been described that the co-culture of two or more cell types influences the cellular behavior. Several authors have evaluated the interaction of co-cultured keratinocytes and fibroblasts.<sup>48,49</sup> In these studies, the presence of fibroblasts in the culture system enhanced the keratinocyte proliferation and differentiation.

In order to improve the system, we created a co-culture of three cell types, *i.e.* HaCaT cells, NHDFs and HSVECs. Both the HaCaT cells and the NHDFs were co-cultured on the oppo-

site sides of the membranes, whereas the HSVECs were cultured on the bottoms of the wells of a cell culture plate without physical contact with the membranes. The results obtained *via* the immunostaining of cytokeratin 14 and type I collagen showed that the number of both HaCaT and NHDF cells in the presence of HSVECs was higher on the PCL-PVA + PL membranes than on the PCL-PVA membranes (Fig. 9). In both cases, the cells grew in co-culture for 7 days without showing any cytotoxic effect. For fibroblasts, the cells were able to form a monolayer on PCL-PVA + PL, although a small number of free spaces were observed on PCL-PVA. A similar trend was observed for the keratinocytes that grew in islands positive for the basal type of cytokeratin (cytokeratin 14). The area of the membrane covered by HaCaT cells was significantly reduced when all three cell types were co-cultured compared to the monocultures of HaCaT cells on the PCL-PVA membranes. However, no significant differences were observed for PCL-PVA + PL (Fig. 9C). This effect could be explained by the use of the mixed medium of DMEM and EGM-2, instead of DMEM alone with a higher serum concentration. One of the main problems related to co-cultured systems is the culture medium requirements. Each cell type needs a specific cell culture medium with different amounts of serum and/or growth factors. In addition, the consumption of such nutrients is higher when the cells are co-cultured. The differences observed in terms of the area covered by keratinocytes between PCL-PVA + PL and PCL-PVA membranes were attributed to the presence of PL,



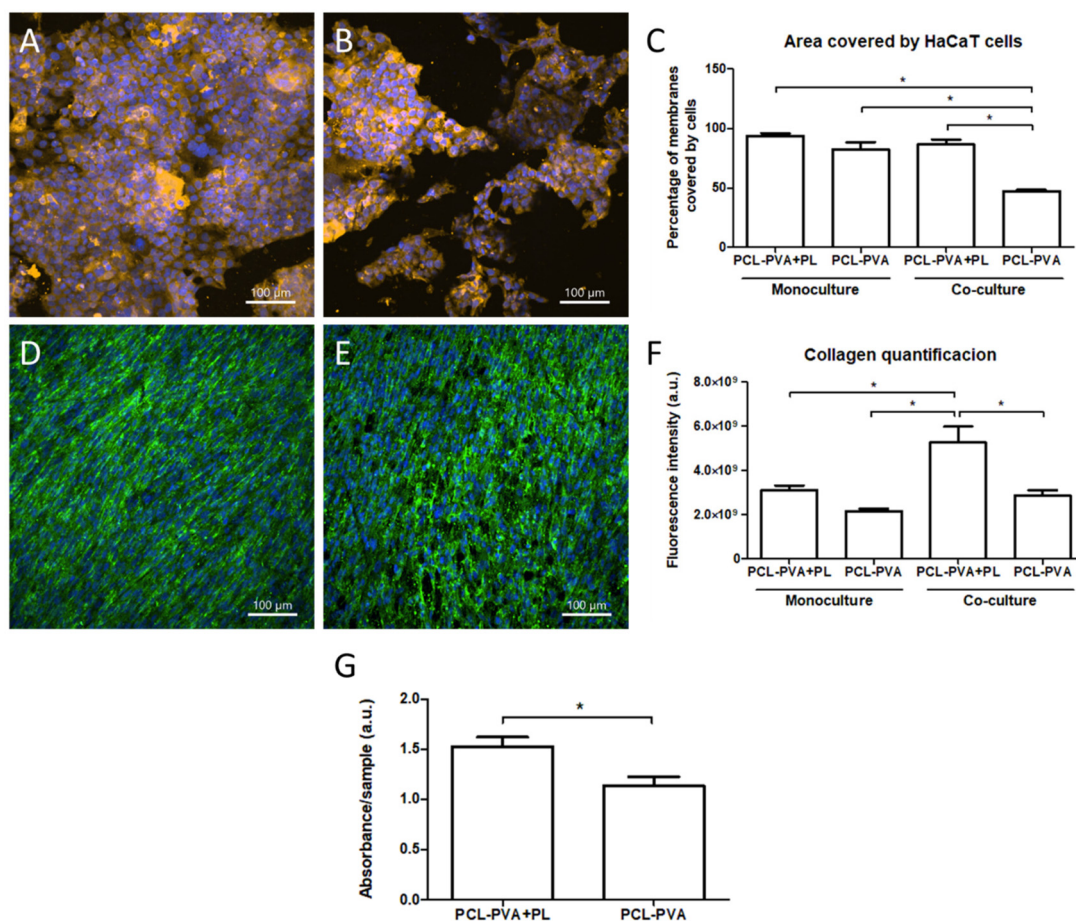


**Fig. 9** HaCaT cells and NHDFs co-cultured on PCL-PVA + PL (A and D) and on PCL-PVA (B and E) nanofibrous membranes with HSVECs for 7 days. Images of the cells stained with cytokeratin 14 (gold) (A and B), with type I collagen (green) (D and E) and with Hoechst (blue); Andor Dragonfly 503 spinning disk confocal microscope equipped with a Zyla 4.2 PLUS sCMOS camera. Quantification of the area covered with HaCaT cells (C) and the type I collagen synthesized by NHDFs (F). Metabolic activity of HaCaT cells and NHDFs that grew on the PCL-PVA + PL or PCL-PVA nanofibrous membranes in co-culture with HSVECs for 7 days (G). The asterisks indicate significant differences ( $p < 0.05$ ).

which compensated the consumption of nutrients in co-cultures. In this regard, our *in vitro* system for co-culturing the three cell types allowed cell proliferation without direct contact among the cell types. Spatial compartmentation of the cells and direct contact of keratinocytes and fibroblasts with the membrane, and indirect contact with the endothelial cells, was the main goal of the co-culture system. We were thus able to develop a system to mimic the *in vivo* conditions with three of the main cell types involved in skin wound healing.

The phenotypic maturation of the fibroblasts was evaluated by quantifying the immunostaining of type I collagen after 7 days of cultivation in both monoculture and co-culture systems (Fig. 9F). No significant differences in fluorescence intensity were found between PCL-PVA + PL and PCL-PVA membranes in monocultures, although a clear increase was observed when the membranes were used for co-cultures. In addition, the co-cultured fibroblasts increased the production of type I collagen compared to the monocultured fibroblasts. These results demonstrate the synergic effect of PL and the presence of keratinocytes and endothelial cells on the fibroblast activity.

The confocal images of HaCaT and NHDF cells corroborated the metabolic activity results. The metabolism or proliferation of both HaCaT cells and NHDFs was significantly higher on the PCL-PVA + PL membranes than on the PCL-PVA membranes (Fig. 9G). In these experiments, the metabolic activity was measured on both cell types at the same time, so these differences could be either due to one cell type or due to both. The results clearly demonstrated that the addition of PL to the nanofibrous membranes had an influence on the keratinocyte and fibroblast behavior. No positive effect of PL on keratinocytes was observed when the cells were monocultured. We therefore hypothesize that the fibroblast activity is responsible for the increase in keratinocyte proliferation. Similar results have been observed by other authors, where keratinocytes and fibroblasts were co-cultured on Ti-based materials.<sup>48</sup> This effect could be related to the expression of nidogen and keratinocyte growth factor (KGF). Nidogen is a component of the basement membrane secreted by fibroblasts, and KGF is produced *via* fibroblast–keratinocyte paracrine interaction, and enhances keratinocyte proliferation.<sup>50,51</sup>



The effect of co-cultivation of the three cell types on the behavior of the HSVECs was also analyzed. The metabolic activity was measured after transferring the membrane with HaCaT cells and NHDFs to another cell culture plate. The results showed that significant differences between PCL-PVA + PL and PCL-PVA nanofibrous membranes in terms of metabolic activity were observed for monocultures of HSVECs. However, no significant differences were observed for the co-cultures (Fig. 10A). The results for monocultures showed the same trend as for the fibroblasts. The presence of PL enhanced the proliferation of endothelial cells. Previous studies have demonstrated that nanomats containing PL supported HSVEC growth to a greater extent than nanomats without PL.<sup>35,36</sup> Regarding the co-cultures, less metabolic activity was observed compared to the monocultures. As explained above, this was potentially caused by the reduced availability of nutrients due to the high consumption of such nutrients by the other two cell types.

The maturation status of the HSVECs was analyzed *via* immunostaining of the von Willebrand factor on day 7 following seeding. The staining pattern of the HSVECs appeared to

be similar for both assessed membranes, with no clear differences between them for either the monocultures or the co-cultures (Fig. 10B–E). The von Willebrand factor is a marker of phenotypic maturation, which plays a role in the adhesion of platelets to the vascular wall and the wound site.<sup>52</sup> The similar staining for the von Willebrand factor indicated that the enhanced proliferation or the presence of other cell types did not interfere with the endothelial cell maturation process. Taking together the results for the endothelial cells, the analyzed membranes did not show any deleterious effect, even enhancing the proliferation of HSVECs when these cells were monocultured in the presence of PCL-PVA + PL nanofibrous membranes.

### 3.5. Effect of platelet lysate released from nanofibrous membranes on fibroblast and endothelial cell migration

The migration of NHDFs was measured 8 hours after the creation of a scratch wound in confluent cell cultures. The results indicated that NHDFs increased their migration when cultured in the presence of PCL-PVA + PL compared to PCL-PVA nanofi-

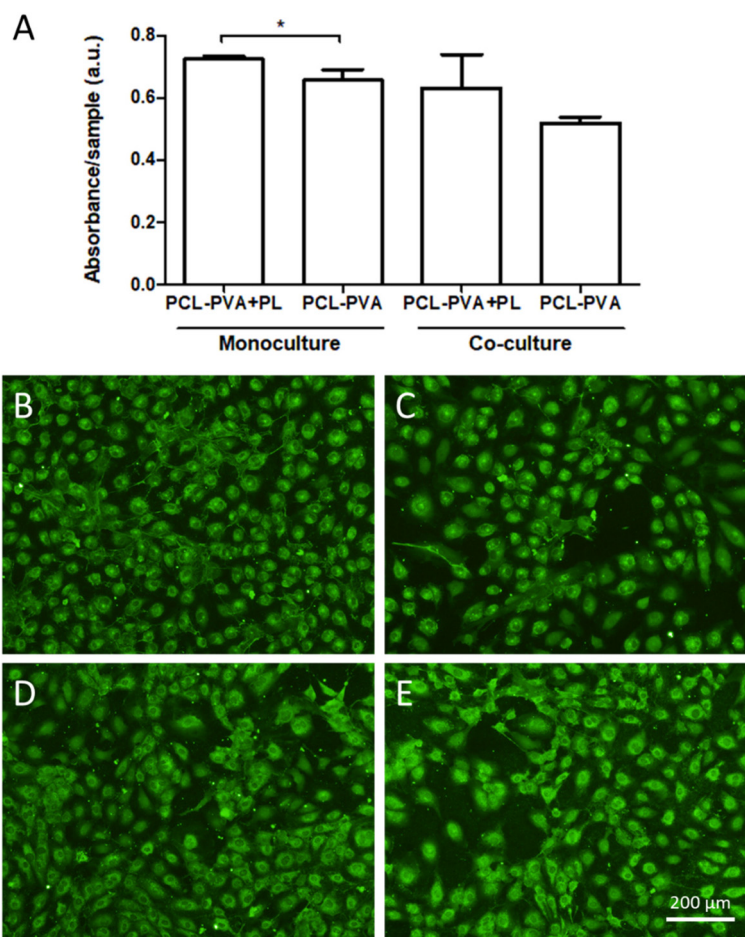


**Fig. 10** Metabolic activity of the HSVECs that grew in the presence of the PCL-PVA + PL and PCL-PVA nanofibrous membranes in monoculture and co-culture for 7 days (A). The asterisks indicate significant differences ( $p < 0.05$ ). HSVECs that grew in the presence of PCL-PVA + PL (B and D) and PCL-PVA (C and E) nanofibrous membranes in monoculture (B and C) or co-cultured (D and E) with HaCaT cells and NHDFs on day 7 after seeding. Images of cells stained for von Willebrand factor (green); Olympus IX50 microscope equipped with a DP70 digital camera, obj. x10.



brous membranes. In addition, NHDFs grown in the presence of PCL-PVA showed an increased level of wound closure compared to the negative control without any membrane (Fig. 11A).

The HSVEC migration towards the nanofibrous membranes was performed using a transmigration assay with inserts. After 4 hours in the culture, the number of HSVECs that crossed the insert membrane was significantly higher in the wells with PCL-PVA + PL nanofibrous membranes than in the PCL-PVA nanofibrous membranes and in the controls (Fig. 11B). The addition of PL enhanced the migration of HSVECs and acted as a chemoattractant.

The migration of fibroblasts and endothelial cells is crucial to the wound-healing process. Fibroblasts proliferate and migrate during the re-epithelization stage. In this phase, the keratinocytes and fibroblasts are stimulated to migrate due to the growth factors released at the wound site. During this process, the basement membrane, epidermal and dermal layers are re-established.<sup>2</sup> In parallel, the formation of new capillaries *via* angiogenesis starts at the injured site. The migration of endothelial cells is therefore essential to ensure the wound healing process. The presence of the vasculature provides nutrients, oxygen, and other cells important for the recovery and maintenance of the skin. Specifically in chronic wounds, angiogenesis is reduced, as well as the capacity of keratinocytes and fibroblasts to migrate to the wound site.<sup>53</sup> In this regard, the PCL-PVA + PL nanofibrous membrane enhanced the migration of fibroblasts and endothelial cells. The incorporation of PL into the nanofibrous membrane and the release of PL into the medium acted as a chemoattractant, which could play an important role in healing chronic wounds.

Chronic wounds often exhibit increased levels of specific biomolecules and enzymes in their exudate, including MMP2, MMP9, IL-1, TNF- $\alpha$ , and many other molecules, along with the presence of bacteria. This complex composition of chronic wound exudate poses challenges for effective wound healing. Studies have shown that chronic wound exudate can hinder

the proliferation and migration of adipose tissue stem cells, and can stimulate the expression of MMP9 in these cells.<sup>54</sup> In addition, it is now well-established that deficiency in growth factors is one of the critical factors that contributes to the development of chronic wounds.<sup>55</sup> Growth factor deficiencies, including reduced levels of bFGF, PDGF, VEGF, and TGF- $\beta$ , have been reported in chronic pressure ulcers when compared with acute wounds.<sup>56</sup> In the present study, the PCL-PVA + PL membranes allowed the protein release from PVA nanofibers. The results showed that PCL-PVA + PL membranes were able to stimulate the metabolic activity and migration of fibroblasts, as well as the transmigration of endothelial cells *in vitro*. When used *in vivo* on chronic wounds, the proteins will be exposed to proteolytic enzymes in the wound exudate and they will be partially degraded. Thus, the action of growth factors and other proteins will be reduced. The balance between protein release and degradation will influence the final growth factor concentration and their effect. Our strategy uses PL as a source of growth factors, cytokines, other bioactive molecules and ions. The concentration of three growth factors present in the PL was previously determined by our research group.<sup>36</sup> In this regard, several authors have studied the effect of platelet-rich plasma and PL to treat wounds with interesting results.<sup>57</sup>

The use of PL and growth factors has been tested in patients in several clinical trials. Human PL was used to treat chronic diabetic foot ulcers with a superior therapeutic effect and without any serious adverse effects.<sup>58</sup> In addition, a meta-analysis of randomized controlled trials demonstrated the efficiency and safety of platelet-rich plasma to treat chronic wounds.<sup>59</sup> Specifically, a clinical trial involving 70 patients with chronic ulcers analyzed the effect of platelet-rich plasma gel. Results showed a reduction in the average wound area when platelet-rich plasma was used.<sup>60</sup> Regarding the use of growth factors, PDGF-BB formulated in gel (Regranex; Johnson and Johnson) is the only growth factor approved by FDA and EMA for wound healing applications.

The effectiveness of exogenous growth factors in wound therapy is contingent upon their spatial and temporal distri-

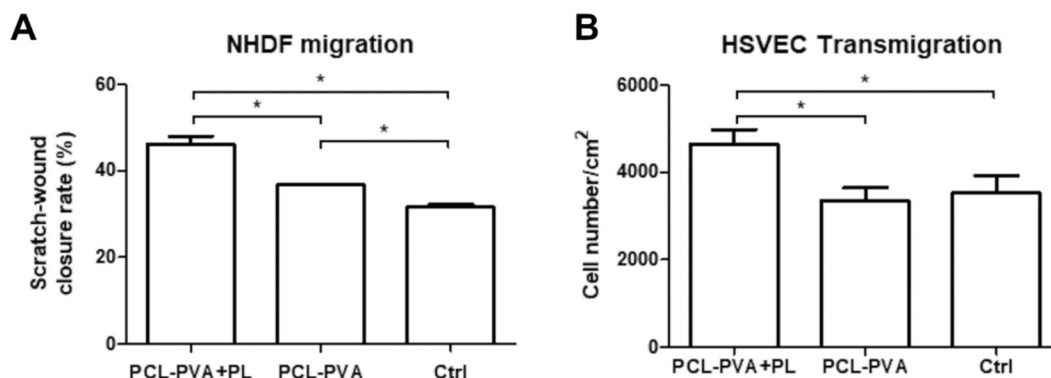


**Fig. 11** (A) Wound closure rate of NHDFs grown in the presence of the PCL-PVA + PL and PCL-PVA nanofibrous membranes, and without membranes (Ctrl) 8 h after a scratch wound was created. (B) The number of HSVECs that transmigrated through the pores of the inserts towards the medium with the PCL-PVA + PL and PCL-PVA nanofibrous membranes, and without membranes (Ctrl) over 4 hours. The asterisks indicate significant differences ( $p < 0.05$ ).



bution within the wound. As previously mentioned, the PL was incorporated into PVA nanofibers serving as a drug delivery system for continuous release of bioactive compounds. The results obtained in the present study using *in vitro* analyses demonstrate the potential of the membranes as a therapeutic wound treatment. Indeed, we hypothesized that both dissolved PVA and albumin in platelet lysate may have a protective effect against proteolysis when used *in vivo*. Nevertheless, wounds differ from each other in production and quantity of wound exudate. Considering the critical role of sustained release and considering the susceptibility of PL to enzymatic degradation in the wound bed, further *in vivo* experiments would be optimum to analyze the effectiveness of wound healing in time.

## 4. Conclusion

A multilayered nanofibrous membrane composed of alternating PCL and PVA layers and allowing the incorporation of PL has been developed as a promising scaffold for skin wound healing. Materials were produced using an original multi-jet needleless electrospinning approach. The biodegradable PCL exhibited suitable properties for cell attachment and growth, and the water-soluble PVA allowed the incorporation of PL. The multilayered nanofibrous membrane acted as a drug delivery system that released bioactive compounds present in PL in effective concentrations. The multilayered membrane without PL (PCL-PVA) and especially the membrane with PL (PCL-PVA + PL) had improved wettability and water absorption compared to PCL, which is important for both *in vitro* and *in vivo* applications.

The multilayered nanofibrous membranes demonstrated their hemocompatibility and cytocompatibility, without deleterious effects for hemolysis and coagulation, and also for the cell adhesion and proliferation of keratinocytes, fibroblasts, and endothelial cells. A co-culture system for three cell types and the nanofibrous membranes has been developed, in which the keratinocytes and fibroblasts were grown on both sides of the membrane, imitating the basement membrane of the skin. The spatial compartmentation allowed the study of paracrine interactions between the cell types.

The bioactivity of the PCL-PVA + PL membranes was demonstrated by increasing the proliferation/cell metabolic activity of the cells compared to the PCL-PVA membranes, and the phenotypic maturation of the fibroblasts was evidenced by type I collagen production. In addition, the migration of fibroblasts and endothelial cells was enhanced by the presence of PCL-PVA + PL membranes. Thus, the beneficial effect of the PCL-PVA + PL multilayered nanofibrous membrane on three cell types involved in wound healing was proved *in vitro*, and the membrane has the potential to treat chronic wounds.

## Conflicts of interest

There are no conflicts to declare.

## Acknowledgements

This study was supported by the Czech Health Research Council, Ministry of Health of the Czech Republic, project NU20-02-00368. Further support was provided by the National Institute for Research of Metabolic and Cardiovascular Diseases project (Programme EXCELES, ID Project No. LX22NPO5104) – Funded by the European Union – Next Generation EU and by the Project No. CZ.02.01.01/00/22\_008/0004562 of the Ministry of Education, Youth and Sports, co-funded by the European Union. Andreu Blanquer has received funding from a postdoctoral fellowship within the Beatriz de Pinós programme, funded by the Secretary of Universities and Research (Government of Catalonia) and by the Horizon 2020 programme of research and innovation of the European Union under Marie Skłodowska-Curie grant agreement No. 801370. We acknowledge the Light Microscopy Core Facility, IMG CAS, Prague, Czech Republic, supported by the Ministry of Education, Youth and Sports of the Czech Republic (LM2018129 Czech-BioImaging), and ERDF (CZ.02.1.01/0.0/0.0/18\_046/0016045) for their support with the confocal imaging.

## References

- 1 S. Sanon, D. A. Hart and E. E. Tredget, *Molecular and Cellular Biology of Wound Healing and Skin Regeneration [Internet]. Skin Tissue Engineering and Regenerative Medicine*. Elsevier Inc., 2016, pp. 19–47. DOI: [10.1016/B978-0-12-801654-1.00002-4](https://doi.org/10.1016/B978-0-12-801654-1.00002-4).
- 2 O. Castaño, S. Pérez-Amodio, C. Navarro-Requena, M. Á Mateos-Timoneda and E. Engel, Instructive microenvironments in skin wound healing: Biomaterials as signal releasing platforms, *Adv. Drug Delivery Rev.*, 2018, **129**, 95–117, DOI: [10.1016/j.addr.2018.03.012](https://doi.org/10.1016/j.addr.2018.03.012).
- 3 M. Martínez-Zapata, A. Martí-Carvajal, I. Solà, J. Expósito, I. Bolívar, L. Rodríguez, *et al.*, Autologous platelet-rich plasma for treating chronic wounds (Review) summary of findings for the main comparison, *Cochrane Database Syst. Rev.*, 2016, (5), CD006899.
- 4 C. K. Sen, G. M. Gordillo, S. Roy, R. Kirsner, L. Lambert, T. K. Hunt, *et al.*, Human skin wounds: A major and snowballing threat to public health and the economy: PERSPECTIVE ARTICLE, *Wound Repair Regen.*, 2009, **17**(6), 763–771.
- 5 J. Holl, C. Kowalewski, Z. Zimek, P. Fiedor, A. Kaminski, T. Oldak, *et al.*, Chronic Diabetic Wounds and Their Treatment with Skin Substitutes, *Cells*, 2021, **10**(3), 1–21.
- 6 J. Yan, G. Tie, S. Wang, A. Tutto, N. Demarco, L. Khair, *et al.*, Diabetes impairs wound healing by Dnmt1-dependent dysregulation of hematopoietic stem cells differentiation towards macrophages, *Nat. Commun.*, 2018, **9**(1), 33.
- 7 P. Borzini and L. Mazzucco, Platelet gels and releasates, *Curr. Opin. Hematol.*, 2005, **12**(6), 473–479.
- 8 P. Martin, Wound healing - Aiming for perfect skin regeneration, *Science*, 1997, **276**(5309), 75–81.





- 9 T. Lim, Q. Tang, Z. Zhu, X. Wei and C. Zhang, Sustained release of human platelet lysate growth factors by thermo-sensitive hydroxybutyl chitosan hydrogel promotes skin wound healing in rats, *J. Biomed. Mater. Res., Part A*, 2020, **108**(10), 2111–2122.
- 10 S. A. Sell, P. S. Wolfe, J. J. Ericksen, D. G. Simpson and G. L. Bowlin, Incorporating Platelet-Rich Plasma into Electrospun Scaffolds for Tissue Engineering Applications, *Tissue Eng., Part A*, 2011, **17**(21–22), 2723–2737.
- 11 W. Cui, Y. Zhou and J. Chang, Electrospun nanofibrous materials for tissue engineering and drug delivery, *Sci. Technol. Adv. Mater.*, 2010, **11**(1), 014108.
- 12 L. Bacakova, M. Zikmundova, J. Pajorova, A. Broz, E. Filova and A. Blanquer, *et al.*, *Nanofibrous Scaffolds for Skin Tissue Engineering and Wound Healing Based on Synthetic Polymers*, in: *Applications of Nanobiotechnology [Internet]*, IntechOpen, 2020. Available from: <https://www.intechopen.com/books/applications-of-nanobiotechnology/nanofibrous-scaffolds-for-skin-tissue-engineering-and-wound-healing-based-on-synthetic-polymers>.
- 13 L. Bacakova, J. Pajorova, M. Zikmundova, E. Filova, P. Mikes and V. Jencova, *et al.*, *Nanofibrous Scaffolds for Skin Tissue Engineering and Wound Healing Based on Nature-Derived Polymers*, in: *Current and Future Aspects of Nanomedicine*, IntechOpen, 2020.
- 14 B. Koprivova, M. Lisnenko, K. Solarska-Sciuk, R. Prochazkova, V. Novotny, J. Mullerova, *et al.*, Large-scale electrospinning of poly (vinylalcohol) nanofibers incorporated with platelet-derived growth factors, *EXPRESS Polym. Lett.*, 2020, **14**(10), 987–1000.
- 15 J. Erben, K. Pilarova, F. Sanetnik, J. Chvojka, V. Jencova, L. Blazkova, *et al.*, The combination of meltblown and electrospinning for bone tissue engineering, *Mater. Lett.*, 2015, **143**, 172–176.
- 16 Q. Zhang, Y. Li, Z. Y. Lin (William), K. K. Y. Wong, M. Lin, L. Yildirim, *et al.*, Electrospun polymeric micro/nanofibrous scaffolds for long-term drug release and their biomedical applications, *Drug Discovery Today*, 2017, **22**(9), 1351–1366.
- 17 Z. Obagi, G. Damiani, A. Grada and V. Falanga, Principles of Wound Dressings: A Review, *Surg. Technol. Int.*, 2019, **10**(25), 50–57.
- 18 S. P. Miguel, D. R. Figueira, D. Simões, M. P. Ribeiro, P. Coutinho, P. Ferreira, *et al.*, Electrospun polymeric nanofibres as wound dressings: A review, *Colloids Surf., B*, 2018, **169**, 60–71.
- 19 S. P. Miguel, R. S. Sequeira, A. F. Moreira, C. S. D. Cabral, A. G. Mendonça, P. Ferreira, *et al.*, An overview of electrospun membranes loaded with bioactive molecules for improving the wound healing process, *Eur. J. Pharm. Biopharm.*, 2019 Jun, **139**, 1–22.
- 20 D. N. Bikiaris, Nanocomposites of aliphatic polyesters: An overview of the effect of different nanofillers on enzymatic hydrolysis and biodegradation of polyesters, *Polym. Degrad. Stab.*, 2013, **98**(9), 1908–1928.
- 21 R. P. Brannigan and A. P. Dove, Synthesis, properties and biomedical applications of hydrolytically degradable materials based on aliphatic polyesters and polycarbonates, *Biomater. Sci.*, 2017, **5**(1), 9–21.
- 22 M. Bartnikowski, T. R. Dargaville, S. Ivanovski and D. W. Hutmacher, Degradation mechanisms of polycaprolactone in the context of chemistry, geometry and environment, *Prog. Polym. Sci.*, 2019, **96**, 1–20.
- 23 Y. Dong, S. Liao, M. Ngiam, C. K. Chan and S. Ramakrishna, Degradation Behaviors of Electrospun Resorbable Polyester Nanofibers, *Tissue Eng., Part B*, 2009, **15**(3), 333–351.
- 24 H. El-Sayed, C. Vineis, A. Varesano, S. Mowafi, R. Andrea Carletto, C. Tonetti, *et al.*, A critique on multi-jet electrospinning: State of the art and future outlook, *Nanotechnol. Rev.*, 2019, **8**(1), 236–245.
- 25 S. A. Hosseini Ravandi, M. Sadrjehani, A. Valipouri, F. Dabirian and F. K. Ko, Recently developed electrospinning methods: a review, *Text. Res. J.*, 2022, **92**, 5130–5145.
- 26 D. Mailley, A. Hébraud and G. Schlatter, A Review on the Impact of Humidity during Electrospinning: From the Nanofiber Structure Engineering to the Applications, *Macromol. Mater. Eng.*, 2021, **306**(7), 2100115.
- 27 S. U. Maheshwari, S. V. Kumar, N. Nagiah and T. S. Uma, Electrospinning of polyvinylalcohol–polycaprolactone composite scaffolds for tissue engineering applications, *Polym. Bull.*, 2013, **70**(11), 2995–3010.
- 28 N. A. Pattanashetti, D. D. Achari, A. I. Torvi, R. V. Doddamani and M. Y. Kariduraganavar, Development of multilayered nanofibrous scaffolds with PCL and PVA: NaAlg using electrospinning technique for bone tissue regeneration, *Materialia*, 2020, **12**, 100826.
- 29 P. Askari, P. Zahedi and I. Rezaeian, Three-layered electrospun PVA/PCL/PVA nanofibrous mats containing tetracycline hydrochloride and phenytoin sodium: A case study on sustained control release, antibacterial, and cell culture properties, *J. Appl. Polym. Sci.*, 2016, **133**(16), 43309.
- 30 M. Ranjbar-Mohammadi, Z. Arab-Bafrani, F. Karimi and N. Javid, Designing hybrid nanofibers based on keratin-poly (vinyl alcohol) and poly ( $\epsilon$ -caprolactone) for application as wound dressing, *J. Ind. Text.*, 2022, **51**(1\_suppl), 1729S–1949S.
- 31 M. S. Salami, G. Bahrami, E. Arkan, Z. Izadi, S. Miraghaee and H. Samadian, Co-electrospun nanofibrous mats loaded with bitter melon (*Momordica charantia*) extract as the wound dressing materials: in vitro and in vivo study, *BMC Complementary Med. Ther.*, 2021, **21**(1), 111.
- 32 A. M. Al-Enizi, M. M. Zagho and A. A. Elzatahy, Polymer-based electrospun nanofibers for biomedical applications, *Nanomaterials*, 2018, **8**, 259.
- 33 M. A. Woodruff and D. W. Hutmacher, The return of a forgotten polymer—Polycaprolactone in the 21st century, *Prog. Polym. Sci.*, 2010 Oct, **35**(10), 1217–1256.
- 34 F. Xu, D. Zou, T. Dai, H.Y Xu, R. An, Y. Liu, *et al.*, Effects of incorporation of granule-lyophilised platelet-rich fibrin into polyvinyl alcohol hydrogel on wound healing, *Sci. Rep.*, 2018, **8**(1), 1–10, DOI: [10.1038/s41598-018-32208-5](https://doi.org/10.1038/s41598-018-32208-5).



- 35 E. Filova, A. Blanquer, J. Knitlova, M. Plencner, V. Jencova, B. Koprivova, *et al.*, The Effect of the Controlled Release of Platelet Lysate from PVA Nanomats on Keratinocytes, Endothelial Cells and Fibroblasts, *Nanomaterials*, 2021, **11**, 995.
- 36 A. Blanquer, J. Musilkova, E. Filova, J. Taborska, E. Brynda, T. Riedel, *et al.*, The Effect of a Polyester Nanofibrous Membrane with a Fibrin-Platelet Lysate Coating on Keratinocytes and Endothelial Cells in a Co-Culture System, *Nanomaterials*, 2021, **11**(2), 457.
- 37 Y. Pan, X. Zhou, Y. Wei, Q. Zhang, T. Wang, M. Zhu, *et al.*, Small-diameter hybrid vascular grafts composed of polycaprolactone and polydioxanone fibers, *Sci. Rep.*, 2017, **7**(1), 3615.
- 38 D. D. Do Pham, V. Jenčová, M. Kaňuchová, J. Bayram, I. Grossová, H. Šuca, *et al.*, Novel lipophosphonoxin-loaded polycaprolactone electrospun nanofiber dressing reduces *Staphylococcus aureus* induced wound infection in mice, *Sci. Rep.*, 2021, **11**(1), 17688.
- 39 M. F. Pucci, P. J. Liotier and S. Drapier, Wicking Tests for Unidirectional Fabrics: Measurements of Capillary Parameters to Evaluate Capillary Pressure in Liquid Composite Molding Processes, *J. Visualized Exp.*, 2017, **119**, e55059.
- 40 E. W. Washburn, The Dynamics of Capillary Flow, *Phys. Rev.*, 1921, **17**(3), 273–283.
- 41 J. Horakova, P. Mikes, A. Saman, T. Svarcova, V. Jencova, T. Suchy, *et al.*, Comprehensive assessment of electrospun scaffolds hemocompatibility, *Mater. Sci. Eng., C*, 2018, **82**, 330–335, <https://linkinghub.elsevier.com/retrieve/pii/S0928493116307913>.
- 42 C. Santos, C. J. Silva, Z. Büttel, R. Guimarães, S. B. Pereira, P. Tamagnini, *et al.*, Preparation and characterization of polysaccharides/PVA blend nanofibrous membranes by electrospinning method, *Carbohydr. Polym.*, 2014, **99**, 584–592.
- 43 M. Jackson and H. H. Mantsch, The Use and Misuse of FTIR Spectroscopy in the Determination of Protein Structure, *Crit. Rev. Biochem. Mol. Biol.*, 1995, **30**(2), 95–120.
- 44 C. Fornaguera and C. Solans, Methods for the In Vitro Characterization of Nanomedicines—Biological Component Interaction, *J. Pers. Med.*, 2017, **7**(1), 2.
- 45 Y. P. Feng, A. Blanquer, J. Fornell, H. Zhang, P. Solsona, M. D. Baró, *et al.*, Novel Fe–Mn–Si–Pd alloys: insights into mechanical, magnetic, corrosion resistance and biocompatibility performances, *J. Mater. Chem. B*, 2016, **4**(39), 6402–6412.
- 46 C. H. Miller, S. J. Platt, A. S. Rice, F. Kelly and J. M. Soucie, Validation of Nijmegen-Bethesda assay modifications to allow inhibitor measurement during replacement therapy and facilitate inhibitor surveillance, *J. Thromb. Haemostasis*, 2012 Jn, **10**(6), 1055–1061.
- 47 N. Raina, R. Pahwa, J. K. Khosla, P. N. Gupta and M. Gupta, Polycaprolactone-based materials in wound healing applications, *Polym. Bull.*, 2022 Sp 8, **79**(9), 7041–7063.
- 48 J. Tan, C. Zhao, J. Zhou, K. Duan, J. Wang, X. Lu, *et al.*, Co-culturing epidermal keratinocytes and dermal fibroblasts on nano-structured titanium surfaces, *Mater. Sci. Eng., C*, 2017, **78**, 288–295, DOI: [10.1016/j.msec.2017.04.036](https://doi.org/10.1016/j.msec.2017.04.036).
- 49 P. Pal, P. Dadhich, P. K. Srivas, B. Das, D. Maulik and S. Dhara, Bilayered nanofibrous 3D hierarchy as skin rudiment by emulsion electrospinning for burn wound management, *Biomater. Sci.*, 2017, **5**(9), 1786–1799.
- 50 S. Werner, Keratinocyte Growth Factor: A Unique Player in Epithelial Repair Processes, *Cytokine Growth Factor Rev.*, 1998, **9**(2), 153–165.
- 51 J. Niu, Z. Chang, B. Peng, Q. Xia, W. Lu, P. Huang, *et al.*, Keratinocyte Growth Factor/Fibroblast Growth Factor-7-regulated Cell Migration and Invasion through Activation of NF- $\kappa$ B Transcription Factors, *J. Biol. Chem.*, 2007, **282**(9), 6001–6011.
- 52 K. S. Sakariassen, P. A. Bolhuis and J. J. Sixma, Human blood platelet adhesion to artery subendothelium is mediated by factor VIII–Von Willebrand factor bound to the subendothelium, *Nature*, 1979, **279**(5714), 636–638, <https://www.nature.com/articles/279636a0>.
- 53 T. Cui, R. S. Kirsner and J. Li, Angiogenesis in Chronic Wounds, in *Advances in Wound Care*, 2010, pp. 347–352.
- 54 P. Koenen, T. A. Spanholtz, M. Maegle, E. Stürmer, T. Brockamp, E. Neugebauer, *et al.*, Acute and chronic wound fluids inversely influence adipose-derived stem cell function: molecular insights into impaired wound healing, *Int. Wound J.*, 2015, **12**(1), 10–16.
- 55 O. Catanzano, F. Quaglia and J. S. Boateng, Wound dressings as growth factor delivery platforms for chronic wound healing, *Expert Opin. Drug Delivery*, 2021, **18**(6), 737–759.
- 56 J. Park, S. Hwang and I. S. Yoon, Advanced Growth Factor Delivery Systems in Wound Management and Skin Regeneration, *Molecules*, 2017, **22**(8), 1259.
- 57 S. Tripathi, K. Soni, P. Agrawal, V. Gour, R. Mondal and V. Soni, Hypertrophic scars and keloids: a review and current treatment modalities, *Biomed. Dermatol.*, 2020 Dc 20, **4**(1), 11.
- 58 H. Alhawari, H. Jafar, M. Al Soudi, L. A. Ameerah, M. Fawaris, M. Saleh, *et al.*, Perilesional injections of human platelet lysate versus platelet poor plasma for the treatment of diabetic foot ulcers: A double-blinded prospective clinical trial, *Int. Wound J.*, 2023, **20**(8), 3116–3122.
- 59 S. Li, F. Xing, T. Yan, S. Zhang and F. Chen, The Efficiency and Safety of Platelet-Rich Plasma Dressing in the Treatment of Chronic Wounds: A Systematic Review and Meta-Analysis of Randomized Controlled Trials, *J. Pers. Med.*, 2023, **13**(3), 430.
- 60 M. H. Mohammadi, B. Molavi, S. Mohammadi, M. Nikbakht, A. M. Mohammadi, S. Mostafaei, *et al.*, Evaluation of wound healing in diabetic foot ulcer using platelet-rich plasma gel: A single-arm clinical trial, *Transfus. Apher. Sci.*, 2017, **56**(2), 160–164.

